

An Inverse Optimization Approach to Measuring Clinical Pathway Concordance

Timothy C. Y. Chan

Department of Mechanical and Industrial Engineering, University of Toronto, Toronto, Ontario M5S3G8, Canada,
 tcychan@mie.utoronto.ca

Maria Eberg, Katharina Forster, Claire Holloway, Luciano Ieraci

Cancer Care Ontario, Toronto, Ontario M5G2C1, Canada, {Maria.Eberg, Katharina.Forster, Claire.Holloway,
 Luciano.Ieraci}@cancercare.on.ca

Yusuf Shalaby, Nasrin Yousefi

Department of Mechanical and Industrial Engineering, University of Toronto, Toronto, Ontario M5S3G8, Canada,
 {yusuf.shalaby, nasrin.yousefi}@mail.utoronto.ca

Clinical pathways outline standardized processes in the delivery of care for a specific disease. Patient journeys through the healthcare system, though, can deviate substantially from recommended or reference pathways. Given the positive benefits of clinical pathways, it is important to measure the concordance of patient pathways so that variations in health system performance or bottlenecks in the delivery of care can be detected, monitored, and acted upon. This paper proposes the first data-driven inverse optimization approach to measuring pathway concordance in any problem context. Our specific application considers clinical pathway concordance for stage III colon cancer. We apply our novel concordance metric to a real dataset of colon cancer patients from Ontario, Canada and show that it has a statistically significant association with survival. Our methodological approach considers a patient's journey as a walk in a directed graph, where the costs on the arcs are derived by solving an inverse shortest path problem. The inverse optimization model uses two sources of information to find the arc costs: reference pathways developed by a provincial cancer agency (primary) and data from real-world patient-related activity from patients with both positive and negative clinical outcomes (secondary). Thus, our inverse optimization framework extends existing models by including data points of both varying "primacy" and "goodness". Data primacy is addressed through a two-stage approach to imputing the cost vector, while data goodness is addressed by a hybrid objective function that aims to both minimize and maximize suboptimality error for different subsets of input data.

Key words: inverse optimization, network flow, clinical pathway concordance, colon cancer, survival analysis

1. Introduction

Clinical pathways, also known as disease pathways or integrated care pathways, are care plans outlining standardized processes in the delivery of care for a specific cohort of patients (Campbell et al. 1998). They prescribe a sequence of steps for managing a clinical process with the aim of

optimizing patient or population-level outcomes such as survival, cost, and wait times. Clinical pathways are widely used across a range of medical domains including cancer (Evans et al. 2013, Schmidt et al. 2018, Ling et al. 2018), mental health (Samokhvalov et al. 2018), and surgical recovery (Van Zelm et al. 2018). With applicability to screening, diagnostic, and treatment processes, they have been shown to be effective in improving patient survival and satisfaction, wait times, in-hospital complications, and cost of care (Rotter et al. 2012, Panella et al. 2003, Schmidt et al. 2018). Given the importance of clinical pathways in promoting best practices and standardizing or streamlining care, there is significant interest in developing quantitative metrics to measure the concordance of patient-traversed pathways against the recommended pathways, which we will refer to as *reference pathways*. Such metrics may assist in monitoring variations in the health system and across the care continuum, identifying bottlenecks or changes in the delivery of care, and ultimately providing data-driven evidence to inform health policy decisions. Understanding the root of any discordance is necessary to fully realize the aforementioned benefits of clinical pathways.

Existing methodologies for measuring similarity between pathways have primarily leveraged process mining, a family of techniques that connect business process management with data mining algorithms (Bose and van der Aalst 2010, Adriansyah et al. 2011, Yang et al. 2017, 2016). General similarity metrics are typically based on edit distance algorithms (van de Klundert et al. 2010, Forestier et al. 2012, Yan et al. 2018), which compare two processes represented as a sequence of distinct activities by counting the minimum number of operations needed to transform one into the other. This type of distance measurement can be weighted, where certain activity deviations are more heavily penalized, or unweighted. Unweighted approaches implicitly assume all deviations are equally disadvantageous, which is limiting since different types of discordance will have differential impact on clinical outcomes. On the other hand, weighted approaches to date have relied on domain knowledge and expert input to determine the weights, which is subjective and sensitive to misspecification. The existing approaches in the literature are either unweighted or use subjectively derived weights. Given these limitations, our focus is on developing a weighted concordance metric with objectively derived or data-driven weights.

There are two sources of information that can be used to derive weights for a concordance metric: reference pathways and data from real-world patient-related activity. We argue that reference pathways should be the primary information source since they are derived from best available medical evidence and are designed for specific clinical outcomes. Furthermore, concordance measurement in a health system is ideally optimized for a hierarchy of outcomes, with clinical outcomes usually given priority. Thus, it makes sense for reference pathways to be used directly to derive weights for the concordance metric. Real-world patient activity, in the form of individual patient pathways, can serve as an important secondary data source to fine tune the weights. However, it should not be

used as a primary source to determine the weights since there can be significant variation between individual patient pathways, and outcomes typically depend on many other contributing and confounding factors besides pathway concordance. Patients with good outcomes may have undertaken activities that are not recommended in the reference pathways or that should not be associated with better outcomes. They may also have missed important activities. Overall, the weights should maximize concordance when a reference pathway is measured against itself while scoring discordant pathways lower. The problem of finding such weights can thus be posed naturally as an inverse optimization problem.

In this paper, our goal is to use inverse optimization to develop a data-driven concordance metric for measuring clinical pathway concordance that has a validated, statistically significant association with patient survival. Such a metric can help pinpoint discordant activity in a complex health system, from geographical regions to individual providers, and therefore support policy makers in crafting informed, data-driven decisions about health system interventions. To support such data-driven decision making, we first need a rigorous approach to measuring concordance.

We model a patient’s journey through the healthcare system as a walk in a directed graph in which each node represents a possible activity that a patient can undertake. Patients incur “costs” by visiting nodes and traversing arcs through the network, which allows us to model both the costs associated with undertaking (or missing) certain activities, as well as sequencing costs for progressing from one activity to the next. A reference pathway can be considered an optimal solution of an appropriately formulated minimum cost network flow problem, a shortest path problem in particular. Given that the “forward” problem is a network flow problem, we can formulate the “inverse” problem tractably using linear programming duality (Ahuja and Orlin 2001). The goal of the inverse optimization model is to find arc costs such that all reference pathways are optimal for the resulting network. If there does not exist a cost vector that makes all reference pathways simultaneously optimal, then the costs should be such that a measure of aggregate error (e.g., optimality gap) is minimized. Once the arc costs are determined, any input pathway (reference or patient-traversed) can be scored based on the cost of the associated directed walk through the network. In other words, these arc costs form the weights used in the concordance metric.

Modern inverse optimization methodologies aim to impute unknown parameters of an optimization problem to make observed decisions minimally suboptimal (Troutt et al. 2006, Keshavarz et al. 2011, Chan et al. 2014, Bertsimas et al. 2015, Aswani et al. 2018, Esfahani et al. 2018, Chan et al. 2019, Babier et al. 2019). Inverse network flow problems are well-studied in the literature, but primarily focus on a single, noiseless observed decision for which it is possible to determine parameters that make the decision exactly optimal (Burton and Toint 1992, Xu and Zhang 1995,

Zhang et al. 1995, Zhang and Ma 1996, Yang et al. 1997, Burton et al. 1997, Zhang and Cai 1998, Ahuja and Orlin 2001, 2002). Inverse network flow problems with multiple noisy observations have received limited attention to date (Faragó et al. 2003, Zhao et al. 2015). We extend these papers by introducing a general inverse optimization framework for standard form linear optimization problems that explicitly accounts for the lower dimensionality of the feasible region due to the equality constraints corresponding to flow balance. This dimensionality issue also requires modifying how goodness-of-fit is measured in inverse optimization, which to date has only considered problems with full dimensional feasible regions (Chan et al. 2019). Finally, unlike many previous papers, we do not restrict the sign of the cost vector.

For a practical application of our inverse optimization framework, we study clinical pathway concordance for stage III colon cancer pathways developed by Cancer Care Ontario. Cancer Care Ontario is the Ontario government’s principal advisor on cancer care. It directs and oversees health-care funds for hospitals and other cancer care providers, enabling them to deliver high-quality, timely services and improved access to care. As such, Cancer Care Ontario’s responsibilities include developing guidelines and standards related to the delivery of cancer care, as well as monitoring the performance of the cancer system in Ontario, Canada. Colon cancer is one of the most commonly diagnosed cancers and a leading cause of death from cancer worldwide for both men and women (World Cancer Research Fund 2019). In our numerical experiments, we demonstrate how inverse optimization can be used to learn a cost vector from reference and patient pathways in an appropriately formulated clinical activity network. We develop both a goodness-of-fit metric to measure the quality of the inverse optimization solution, as well as a concordance metric to measure the concordance of individual patient pathways. Finally, we provide a rigorous survival analysis to demonstrate the association of our concordance metric with survival, using a cohort of stage III colon cancer patients. Although we focus on colon cancer specifically in this paper, our inverse optimization-based approach is generalizable to other patient cohorts and even beyond the healthcare context to general process management applications for which data-driven concordance measurement is a critical need.

Our main contributions in this paper are as follows:

1. We propose the first inverse optimization-based approach for measuring pathway concordance in any problem context. Methodologically, our approach differs from previous inverse optimization models with the inclusion of a mixture of both “good” and “bad” data points; that is, points that the optimal cost vector should fit well and points that it should not fit well, respectively. Our approach also considers the novel setup where there is a primary (reference pathways) and secondary (patient pathways) dataset, which should be given differential consideration when imputing the cost vector.

2. We develop two metrics for goodness-of-fit assessment. The first metric extends a previously developed metric for in-sample goodness-of-fit measurement between the decision model, the input data, and the imputed parameters. This metric is tailored to our particular inverse optimization model and considers the lower dimensionality of the feasible region in standard form linear optimization problems such as network flow problems. The second metric, used for out-of-sample measurement, uses the inversely optimized cost vector to calculate a concordance score for a given flow vector (patient pathway). Both metrics are simple to compute and easily interpretable, with intuitive mathematical properties such as taking values between 0 and 1, with 1 representing perfect fit or concordance.

3. We provide an in-depth case study applying our inverse optimization-based models and metrics to real patient data from a cohort of stage III colon cancer patients. We show through a rigorous survival analysis that there is a statistically significant association between the concordance score of patient-traversed pathways and survival, validating the meaningfulness of our concordance metric. We further quantify the value of our data-driven approach by demonstrating that the patient data-driven concordance metric is much more strongly associated with survival than a metric developed using only reference pathways and without access to the patient data.

All proofs are included in the Appendix.

2. Motivating a Graph-Based Inverse Optimization Approach

In this paper, we leverage network optimization and the corresponding graph-based representation of the problem to measure pathway concordance. To motivate our approach, we briefly highlight the differences between edit distance-based methods (Navarro 2001) and our proposed approach. In particular, we show that our approach provides more granularity and modeling flexibility in capturing different types of discordance, and provides a framework that facilitates data-driven estimation of weights.

First, consider unweighted edit distance algorithms, which measure distance as the minimum number of distortions or edits required to transform a source pattern into a target pattern (van de Klundert et al. 2010, Forestier et al. 2012, Yan et al. 2018, Riesen 2015). The edit operations are defined on the activities in the pathway and usually include insertions, deletions, substitutions, and transpositions, although some algorithms may count a transposition as two substitutions. In contrast, our graph-based approach measures distance using the difference in the total cost along the arcs traversed by the two pathways. Note that edit distance has been extended to graph structures where the edit operations are applied to nodes and arcs (Gao et al. 2010). In the context of clinical pathways, the entire graph is simply a path representing the clinical events of interest sequentially in time. A key difference is that graph edit distance compares two pathways represented

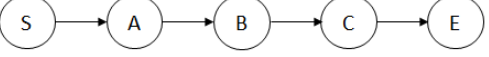
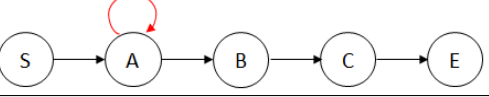
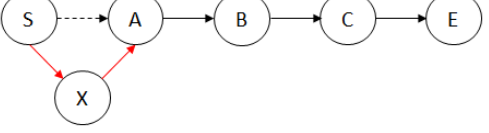
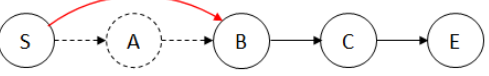
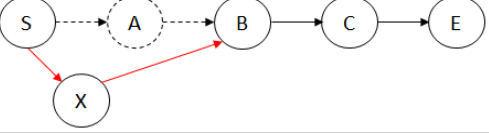
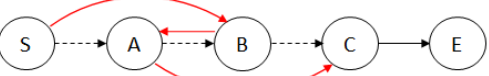
as two distinct graphs, whereas in our approach the two pathways are distinct walks in a single, pre-defined graph.

Our approach improves on edit distance algorithms by better characterizing pathway deviations and optimally estimating weights for those deviations. We refer to arcs that are in a reference pathway as “concordant” if they connect the desired activities in the order indicated according to clinical guidelines. In contrast, “discordant” arcs are those that do not connect activities contained in the reference pathways, or connect such activities out of sequence. The concordance of an observed pathway is then a function of the discordant arcs present and the concordant arcs absent.

To illustrate the ability of our algorithm to better characterize pathway variation, we present concrete examples shown in Table 1. Consider a network with an artificial start node S and end node E that bookend all pathways and let $A - B - C$ be a reference pathway represented by the sequence of arcs (S, A) , (A, B) , (B, C) and (C, E) . Now consider five example pathways listed in Table 1, all of which have the same edit distance of one from $A - B - C$. We can see that despite having the same edit distance, these pathways have different numbers of concordant and discordant arcs. Concordance measurement based on absence of concordant arcs and presence of discordant arcs implies that each pathway can have a different graph-based distance from the reference pathway. Furthermore, when considering pathways with an edit distance of two or more from the reference pathway, differences with graph-based distance measurement are magnified. For example, two adjacent deletions are different from two nonadjacent deletions in terms of the number of concordant and discordant arcs.

The preceding discussion assumes that all arcs and operations (in the edit distance setting) are unweighted. If we now consider a weighted distance metric, an issue arises where the cost of edits would need to be determined a priori and exogenously from our reference pathways. In weighted edit distance, weights or costs are associated with each type of operation. The distance between pathways then becomes the minimum cost of edit operations required to transform one into the other. Determining the costs of each operation based on a set of reference and non-reference pathways is complicated by the dependency of the edits on the costs. Expectation maximization can be used, but this approach does not guarantee convergence to a global optimum (Neuhaus and Bunke 2004, Ristad and Yianilos 1998). In contrast, our inverse optimization approach avoids this dependency and can determine optimal costs for each arc by assuming pathways are optimal solutions to an appropriately formulated optimization problem. The ability to optimally infer arc costs or weights, together with finer characterization of pathway variation using concordant and discordant arcs, are the main strengths of our inverse optimization approach.

Table 1 Comparing concordant and discordant arcs in pathways that have edit distance of one from the reference pathway

Pathway	Edit operation	Missing concordant arcs	Extra discordant arcs	Pathway representation
A-B-C	-	0	0	
A-A-B-C	Insertion (duplicated activity)	0	1	
X-A-B-C	Insertion (discordant activity)	1	2	
B-C	Deletion	2	1	
X-B-C	Substitution	2	2	
B-A-C	Transposition	3	3	

Notes. Missing concordant arcs are dashed. Extra discordant arcs are red.

3. Inverse Optimization for Pathway Concordance Measurement

In this section, we first present a model of the clinical activity network representing all the activities that a cancer patient can undertake during his or her cancer care journey. A patient journey is modeled as a walk through the network. We assume that each arc incurs a cost when a patient takes that arc and that the reference pathways are optimal solutions with respect to an appropriate optimization problem defined on this network. Our goal is to find the costs on each arc and to use it to measure the concordance of a given pathway to the reference pathways.

3.1. The Clinical Activity Network

Let \mathcal{N} be a set of m nodes and let $\mathcal{A} \subseteq \mathcal{N} \times \mathcal{N}$ be a set of n directed arcs in the network. Nodes represent clinical activities that can be undertaken by a patient. To model the cost of undertaking a specific activity i , we split each activity node into two nodes, i_s and i_e , representing the start and end, respectively, of activity i , and then add an arc (i_s, i_e) with cost $c_{i_s i_e}$. The remaining arcs connect the end node of some activity i with the start node of another activity j . Each arc

(i_e, j_s) has an associated cost $c_{i_e j_s}$, representing the cost of undertaking activity j immediately after activity i . The set \mathcal{A} also includes arcs of the form (i_e, i_s) , which allows the network to model a patient journey that involves consecutive repetitions of activity i . Finally, we add two artificial nodes representing the common start and end of each patient journey. Thus, m is equal to two times the number of clinical activities plus two.

A reference pathway is represented as the solution of a shortest path problem on this network. We write this shortest path problem as a standard form linear optimization problem representing the corresponding network flow model: $\min_{\mathbf{x}} \{ \mathbf{c}' \mathbf{x} : \mathbf{Ax} = \mathbf{b}, \mathbf{x} \geq \mathbf{0} \}$. We denote this model the “forward” model and will refer to it as $\mathbf{FO}(\mathbf{c})$. The decision vector $\mathbf{x} \in \mathbb{R}^n$ describes the flow on each arc. The matrix $\mathbf{A} \in \mathbb{R}^{(m-1) \times n}$ is the node-arc incidence matrix, but without the m th row, which corresponds to the flow balance constraint of the artificial end node. Thus, it is full rank. The parameter $\mathbf{b} \in \mathbb{R}^{m-1}$ is a vector of zeros except with a $+1$ at the artificial start node.

A patient journey will be represented as a walk on this network. Note that it may not necessarily be a path since patients may visit an activity or traverse an arc several times. Thus, a patient journey through the network can still be represented by a flow vector $\mathbf{x} \in \mathbb{R}^n$, except that the value of x_{ij} may be greater than one, representing the number of times arc (i, j) is traversed in the corresponding walk. In keeping with the medical terminology, we will refer to a patient journey as a patient “pathway”, which in general should be thought of as a walk through the network. We will reserve the use of the phrase “path” for the mathematical concept of a walk without repeated nodes.

Note that with the current setup, costs are “path-independent”. That is, the cost of traversing arc (i, j) is equal to c_{ij} regardless of how the walk arrives at node i . To model path-dependent costs, where the cost of completing activity j immediately following activity i depends on what activities were completed prior to i , we could modify the nodes in the network from representing a single activity to representing the sequence of activities from the artificial start node to the current activity. That is, imagine a network organized in “layers”, where the first layer of nodes comprises all activities that can be reached from the start node in one step, the second layer of nodes comprises all sequences of activities that can be reached in two steps, etc. While the cost-dependent approach provides richer modeling possibilities, the downside is an exponential explosion in the number of nodes in the network. Thus, we proceed with the network as currently defined (i.e., with path-independent costs) to maintain a parsimonious model, and instead integrate path-dependent behavior into the constraints of the inverse optimization model, which is described next.

3.2. Inverse Optimization Model

Our goal is to identify a cost vector $\mathbf{c} \in \mathbb{R}^n$ that minimizes the aggregate suboptimality of given reference pathways, assuming they represent shortest paths. We first present a basic inverse optimization model that provides an exact formulation of this problem. Then, we introduce a second

formulation that uses patient pathways to refine the optimal cost vector returned by the first model, in order to improve the association between pathway concordance and survival.

3.2.1. A Model Using Only Reference Pathways. Let $\hat{\mathcal{X}}^r = \{\hat{\mathbf{x}}_1^r, \dots, \hat{\mathbf{x}}_R^r\}$ denote the set of R reference pathways, each assumed to be feasible flow vectors for the forward problem. We follow a standard approach to formulating the inverse optimization problem using duality of linear optimization. Let $\mathbf{p} \in \mathbb{R}^{m-1}$ be the dual vector associated with flow balance constraints. The following formulation is an inverse optimization model that minimizes the sum of squared absolute duality gaps induced by the cost vector \mathbf{c} and the R reference pathways:

$$\begin{aligned} \mathbf{IO}^{\text{ref}}(\hat{\mathcal{X}}^r): \quad & \underset{\mathbf{c}, \mathbf{p}, \epsilon^r}{\text{minimize}} \quad \sum_{q=1}^R (\epsilon_q^r)^2 \\ & \text{subject to} \quad \mathbf{A}'\mathbf{p} \leq \mathbf{c}, \\ & \quad \mathbf{c}'\hat{\mathbf{x}}_q^r = \mathbf{b}'\mathbf{p} + \epsilon_q^r, \quad q = 1, \dots, R, \\ & \quad \|\mathbf{c}\|_\infty = 1, \\ & \quad \mathbf{A}\mathbf{c} = \mathbf{0}. \end{aligned} \tag{1}$$

The first constraint represents dual feasibility. The second constraint defines the duality gap ϵ_q^r for each reference pathway $\hat{\mathbf{x}}_q^r$ as the difference between the primal and dual objective values. Each duality gap variable is nonnegative since the reference pathways are feasible for the forward problem. The third constraint is a normalization constraint to ensure the cost vector is not trivial (i.e., non-zero). The fourth constraint is needed to ensure that \mathbf{c} lies in the lower dimensional space defined by the constraints $\mathbf{Ax} = \mathbf{b}$. Since \mathbf{c} lies in the space defined by the intersection of the equality constraints ($\mathbf{a}_i' \mathbf{x} = b_i, i = 1, \dots, m-1$), it must be orthogonal to the vectors defining those constraints (\mathbf{a}_i). Without the constraint $\mathbf{Ac} = \mathbf{0}$, an optimal solution (i.e., cost vector) to formulation (1) could be orthogonal to the entire forward feasible region, which would render \mathbf{c} uninformative since every feasible flow vector would be optimal. To our knowledge, the issue of finding an optimal cost vector via inverse optimization for a lower dimensional feasible region (which is characteristic of any inverse network flow problem) has not been studied in the inverse optimization literature previously. Note that the constraint $\mathbf{Ac} = \mathbf{0}$ means that the optimal cost vector will be a circulation.

To model additional application-specific considerations, such as user-specified rankings between certain activities or preferences for how a patient should begin or end her pathway, we will add a set of constraints on the cost vector, $\mathbf{c} \in \mathcal{C}$, to formulation (1). Specific examples of such constraints are provided in Section 5.

First, we prove that formulation (1) has an optimal solution for any non-trivial network.

LEMMA 1. $\mathbf{IO}^{\text{ref}}(\hat{\mathcal{X}}^r)$ has an optimal solution if and only if there are at least two distinct paths from the start node to the end node.

Given Lemma 1, we assume going forward that the network is non-trivial (i.e., more than a single path) and $\mathbf{IO}^{\text{ref}}(\hat{\mathcal{X}}^r)$ always has an optimal solution. Next, we present an important property of an optimal solution to $\mathbf{IO}^{\text{ref}}(\hat{\mathcal{X}}^r)$.

PROPOSITION 1. Let $(\mathbf{c}^*, \mathbf{p}^*, \boldsymbol{\epsilon}^{r*})$ be an optimal solution to formulation (1). Then, the network with arc costs \mathbf{c}^* does not contain any directed negative cost cycles.

This result has an intuitive real-world interpretation. It says that a patient traversing the cancer care network cannot accrue a positive benefit through repeating any sequence of activities. This will certainly be the case if the outcome is measured in terms of monetary cost of the activities. But even viewed through the lens of survival, it makes sense that such negative cost cycles do not exist. Otherwise, there would be a sequence of activities that guarantees improved survival, which is not realistic. We also note that a finite optimal value for (1) is important for the goodness-of-fit and concordance metrics, which we define later.

Formulation (1) is non-convex because of the normalization constraint. However, it can be solved using polyhedral decomposition: solving $2n$ quadratic optimization problems where the normalization constraint is replaced with $c_{ij} \in [-1, 1]$ for all $(i, j) \in \mathcal{A}$ and with one additional constraint on one c_{ij} being set to either $+1$ or -1 :

$$\begin{aligned} \mathbf{IO}_{ij}^{\text{ref}}(\hat{\mathcal{X}}^r) : \quad & \underset{\mathbf{c}, \mathbf{p}, \boldsymbol{\epsilon}^r}{\text{minimize}} \quad \sum_{q=1}^R (\epsilon_q^r)^2 \\ & \text{subject to} \quad \mathbf{A}'\mathbf{p} \leq \mathbf{c}, \\ & \quad \mathbf{c}'\hat{\mathbf{x}}_q^r = \mathbf{b}'\mathbf{p} + \epsilon_q^r, \quad q = 1, \dots, R, \\ & \quad c_{ij} = -1 \vee c_{ij} = 1, \\ & \quad -1 \leq c_{ij} \leq 1, \quad (i, j) \in \mathcal{A}, \\ & \quad \mathbf{A}\mathbf{c} = \mathbf{0}. \end{aligned} \tag{2}$$

Furthermore, if in a particular problem context it is clear which arc should be either the most heavily rewarded (set $c_{ij} = -1$) or heavily penalized (set $c_{ij} = +1$), then only one of these $2n$ problems needs to be solved. As we demonstrate later, this is the case for our clinical problem.

3.2.2. Refining the Solution using Patient Data. Let $\hat{\mathcal{X}}^s = \{\hat{\mathbf{x}}_1^s, \dots, \hat{\mathbf{x}}_S^s\}$ denote a dataset of S patient pathways with good clinical outcomes (i.e., survived) and $\hat{\mathcal{X}}^d = \{\hat{\mathbf{x}}_1^d, \dots, \hat{\mathbf{x}}_D^d\}$ denote a dataset of D patient pathways with poor clinical outcomes (i.e., died), all assumed to be feasible flow vectors for the forward problem. If formulation (1) has multiple optimal solutions, we can

use these two datasets to determine a cost vector that not only maximizes fit with the reference pathways, but also provides “separation” between $\hat{\mathcal{X}}^s$ and $\hat{\mathcal{X}}^d$. Once formulation (1) is solved and an optimal duality gap vector, ϵ^{r*} , is generated, we use ϵ^{r*} as input into the following inverse optimization model:

$$\begin{aligned}
 \mathbf{IO}^{\text{pat}}(\hat{\mathcal{X}}^s, \hat{\mathcal{X}}^d, \epsilon^{r*}) : \quad & \underset{\mathbf{c}, \mathbf{p}, \epsilon^s, \epsilon^d}{\text{minimize}} \quad \frac{D}{S} \sum_{q=1}^S \epsilon_q^s - \sum_{q=1}^D \epsilon_q^d \\
 & \text{subject to} \quad \mathbf{A}' \mathbf{p} \leq \mathbf{c}, \\
 & \mathbf{c}' \hat{\mathbf{x}}_q^r = \mathbf{b}' \mathbf{p} + \epsilon_q^{r*}, \quad q = 1, \dots, R, \\
 & \mathbf{c}' \hat{\mathbf{x}}_q^s = \mathbf{b}' \mathbf{p} + \epsilon_q^s, \quad q = 1, \dots, S, \\
 & \mathbf{c}' \hat{\mathbf{x}}_q^d = \mathbf{b}' \mathbf{p} + \epsilon_q^d, \quad q = 1, \dots, D, \\
 & \|\mathbf{c}\|_\infty = 1, \\
 & \mathbf{A} \mathbf{c} = \mathbf{0}.
 \end{aligned} \tag{3}$$

Since data from $\hat{\mathcal{X}}^s$ represents “good” data, we treat it like input to traditional inverse optimization models (and like the reference pathways), where the goal is to minimize the aggregate suboptimality of these data points. However, since $\hat{\mathcal{X}}^d$ consists of “bad” data points, we do not want to learn a cost vector that fits this data well. Instead, the cost vector should generate data points as far away as possible from those in $\hat{\mathcal{X}}^d$ when solving the forward problem, which is why in formulation (3) the objective maximizes suboptimality with respect to $\hat{\mathcal{X}}^d$. The weight D/S simply scales the two sub-objectives to account for the difference in the number of data points in the two groups. The second constraint forces the cost vector to achieve the optimal duality gap found in model (1). In other words, all feasible solutions of (3) are optimal solutions to (1). The third and fourth constraints define the duality gaps with respect to the pathways in $\hat{\mathcal{X}}^s$ and $\hat{\mathcal{X}}^d$, respectively. Again, the duality gaps are nonnegative since all patient pathways are feasible for the forward problem. The remaining constraints are as defined in (1). Formulation (3) can be solved using the same polyhedral decomposition technique described previously. The difference is that each subproblem is a linear optimization problem, since the objective function is now linear. A linear objective was chosen for formulation (3) to facilitate the combination of duality gaps that needed to be minimized and maximized in the same objective.

Next, we establish that formulation (3) will always return an optimal cost vector.

PROPOSITION 2. $\mathbf{IO}^{\text{pat}}(\hat{\mathcal{X}}^s, \hat{\mathcal{X}}^d, \epsilon^{r*})$ has an optimal solution.

In our numerical results, we implement two slightly different versions of formulation (3). In Section 6, we visualize the solution of our inverse optimization model (i.e., the cost vector) and

compute goodness-of-fit using all of our patient data to form the sets $\hat{\mathcal{X}}^s$ and $\hat{\mathcal{X}}^d$. These results are thus “in-sample”. However, the patient concordance scores in that section and in the survival analysis in Section 7 are computed “out-of-sample”. That is, we use only a subset of the full patient dataset to form $\hat{\mathcal{X}}^s$ and $\hat{\mathcal{X}}^d$ in model (3), and the resulting optimal cost vector \mathbf{c}^* is used to calculate a concordance score for the patients that were not used to determine \mathbf{c}^* . These out-of-sample concordance scores then constitute an independent variable in the survival analysis model.

4. Goodness-of-Fit and Concordance Metrics

In this section, we develop two fitness metrics. The first measures the goodness of fit of the optimal cost vector generated by the inverse optimization model against the input data. The second metric measures the concordance of a given patient pathway against the reference pathways, using the optimal cost vector generated by the inverse optimization model. It should be applied to patient pathways that have yet to be observed and that are not in the “training data” that was used to generate optimal cost vector.

4.1. Goodness-of-Fit of the Cost Vector

We extend a previously developed goodness-of-fit metric for inverse optimization, the *coefficient of complementarity* (Chan et al. 2019), so that it is appropriate for measuring the fitness of cost vectors produced by model (3). The previous metric required the forward feasible region to be full-dimensional, which is not the case here due to the flow balance equality constraints. Our metric is like R^2 in linear regression in that it measures the fit between the input data and the estimated model, and possesses analogous mathematical properties. First, we present a general form of our goodness-of-fit metric that is applicable to any problem, regardless of whether the forward feasible region is full-dimensional, and examine its theoretical properties. Then, we introduce a modified form that is appropriately tailored to the lower-dimensional space in which the forward feasible region resides.

Since our primary goal is to find a cost vector that fits the reference pathways, and since model (3) simply searches among the optimal cost vectors for one that separates patients with good and bad outcomes, we focus on measuring model-data fit with respect to the reference pathways and not the patient data.

Let \mathbf{c}^* be an optimal cost vector for (3) and $\mathbf{c}_1, \dots, \mathbf{c}_T$ be a set of cost vectors that are feasible for (1). Let \mathbf{x}^* be an optimal solution to $\mathbf{FO}(\mathbf{c}^*)$ and $\mathbf{x}_1, \dots, \mathbf{x}_T$ be defined similarly with respect to $\mathbf{c}_1, \dots, \mathbf{c}_T$. We define the goodness of fit of \mathbf{c}^* with respect to the reference pathways $\hat{\mathcal{X}}^r$ as

$$\rho(\hat{\mathcal{X}}^r) = 1 - \frac{\sum_{q=1}^R (\mathbf{c}^{*'} \hat{\mathbf{x}}_q^r - \mathbf{c}^{*'} \mathbf{x}^*)^2}{\frac{1}{T} \sum_{t=1}^T \left(\sum_{q=1}^R (\mathbf{c}_t' \hat{\mathbf{x}}_q^r - \mathbf{c}_t' \mathbf{x}_t)^2 \right)}. \quad (4)$$

Note that $\mathbf{c}^* \mathbf{x}^*$ and $\mathbf{b}' \mathbf{p}^*$ can be used interchangeably since they represent the optimal primal and dual objective values, respectively, which are equal. Therefore, $\mathbf{c}^* \mathbf{x}_q^r - \mathbf{c}^* \mathbf{x}^* = \epsilon_q^{r*}$. Similarly, each term $\mathbf{c}_t' \hat{\mathbf{x}}_q^r - \mathbf{c}_t' \mathbf{x}_t$ in the denominator is equal to a duality gap for a reference pathway q with respect to the cost vector \mathbf{c}_t .

Next, we show that $\rho(\hat{\mathcal{X}}^r)$ has attractive mathematical properties that facilitate its use and interpretation. Recall that an optimal \mathbf{c}^* for formulation (3) is also optimal for (1). Thus, although Theorem 1 focuses on formulation (1), it is equally applicable to cost vectors generated from model (3). Some additional notation is needed before proceeding. Let $\mathcal{A}_{(k)} \subset \mathcal{A}$ be a set of k arcs from the network, $k = 1, \dots, n-1$. We define

$$\rho_{(k)}(\hat{\mathcal{X}}^r) = 1 - \frac{\sum_{q=1}^R (\mathbf{c}^*_{(k)} \hat{\mathbf{x}}_q^r - \mathbf{c}^*_{(k)} \mathbf{x}^*)^2}{\frac{1}{T} \sum_{t=1}^T \left(\sum_{q=1}^R (\mathbf{c}_t' \hat{\mathbf{x}}_q^r - \mathbf{c}_t' \mathbf{x}_t)^2 \right)},$$

where $\mathbf{c}^*_{(k)}$ is an optimal solution for $\mathbf{IO}_{(k)}^{\text{ref}}(\hat{\mathcal{X}}^r)$, defined as $\mathbf{IO}^{\text{ref}}(\hat{\mathcal{X}}^r)$ with additional constraints $c_{ij} = 0$ for $(i, j) \notin \mathcal{A}_{(k)}$.

THEOREM 1. 1. **Optimality:** $\rho(\hat{\mathcal{X}}^r)$ is maximized by an optimal solution to $\mathbf{IO}^{\text{ref}}(\hat{\mathcal{X}}^r)$.

2. **Boundedness:** $\rho(\hat{\mathcal{X}}^r) \in [0, 1]$.

3. **Monotonicity:** $\rho_{(k)}(\hat{\mathcal{X}}^r) \leq \rho_{(k+1)}(\hat{\mathcal{X}}^r)$ if $\mathcal{A}_{(k)} \subset \mathcal{A}_{(k+1)}$.

Given the reference pathways $\hat{\mathcal{X}}^r$ and an optimal solution \mathbf{c}^* to (1) (or (3)), $\rho(\hat{\mathcal{X}}^r)$ measures the degree to which the reference pathways are shortest paths with respect to \mathbf{c}^* . If all reference pathways are shortest paths with respect to \mathbf{c}^* , then $\rho(\hat{\mathcal{X}}^r) = 1$.

When the forward feasible region is full-dimensional, an appropriate choice for the baseline cost vectors consist of the vectors normal to the constraints defining the feasible region, i.e., the rows of the coefficient matrix \mathbf{A} (Chan et al. 2019). Thus, where it is straightforward to work directly in the lower-dimensional space, we should modify the computation of $\rho(\hat{\mathcal{X}}^r)$ to avoid having to make a subjective choice for $\mathbf{c}_1, \dots, \mathbf{c}_T$. In particular, we can eliminate the equality constraints $\mathbf{Ax} = \mathbf{b}$ by variable substitution (details in Appendix B) and compute the following “full-dimensional” version of $\rho(\hat{\mathcal{X}}^r)$ in dimension $n - (m - 1)$

$$\rho_f(\hat{\mathcal{Z}}^r) = 1 - \frac{\sum_{q=1}^R (\mathbf{c}^* \hat{\mathbf{z}}_q^r - \mathbf{c}^* \mathbf{x}^*)^2}{\frac{1}{n} \sum_{t=1}^n \left(\sum_{q=1}^R (\mathbf{h}_t' \hat{\mathbf{z}}_q^r - b_t)^2 \right)}, \quad (5)$$

where $\hat{\mathcal{Z}}^r = \{\hat{\mathbf{z}}_1^r, \dots, \hat{\mathbf{z}}_R^r\}$ and \mathbf{h}_t defines the t -th inequality constraint defining the feasible region in the lower-dimensional space (i.e., $\mathbf{h}_t' \mathbf{z} \geq b_t$, $t = 1, \dots, n$). Importantly, the properties proved in Theorem 1 hold for $\rho_f(\hat{\mathcal{Z}}^r)$ (Chan et al. 2019). In our numerical results, we project the reference pathways and forward feasible region to the lower-dimensional space and calculate $\rho_f(\hat{\mathcal{Z}}^r)$ when measuring fitness between the optimal cost vector and the reference pathways.

4.2. Concordance of a Patient Pathway

Using the cost vector generated by inverse optimization, our concordance metric $\omega(\hat{\mathbf{x}})$ measures the cost of a patient pathway $\hat{\mathbf{x}}$ against the cost of a shortest path with respect to \mathbf{c}^* as

$$\omega(\hat{\mathbf{x}}) = 1 - \frac{\mathbf{c}^* \hat{\mathbf{x}} - \mathbf{c}^* \mathbf{x}^*}{M(\hat{\mathbf{x}}) - \mathbf{c}^* \mathbf{x}^*} \quad (6)$$

where $M(\hat{\mathbf{x}}) = \max_{\mathbf{x}} \{\mathbf{c}^* \mathbf{x} : \mathbf{A} \mathbf{x} = \mathbf{b}, \mathbf{x} \geq \mathbf{0}, \|\mathbf{x}\|_1 \leq \|\hat{\mathbf{x}}\|_1, \mathbf{x} \text{ is a walk}\}$. In other words, $M(\hat{\mathbf{x}})$ is the cost of a longest walk, which can be determined via dynamic programming (see Appendix C). Note that we use the cost of the shortest path, $\mathbf{c}^* \mathbf{x}^*$, instead of the cost of a reference pathway when measuring concordance. Since a reference pathway may not actually be a shortest path under \mathbf{c}^* , and since there may be multiple reference pathways with different costs under \mathbf{c}^* , we define the concordance metric using $\mathbf{c}^* \mathbf{x}^*$ to have a consistent and objective baseline. Of course, if the inverse optimization model finds a cost vector that perfectly fits all of the reference pathways (i.e., $\rho = 1$), then the cost of all reference pathways will be equal to $\mathbf{c}^* \mathbf{x}^*$, and $\omega(\hat{\mathbf{x}})$ will be measuring concordance directly against the cost of the reference pathways.

Next, we show that $\omega(\hat{\mathbf{x}})$ has the attractive property of being a unitless metric between 0 and 1, with 1 representing a perfectly concordant pathway (i.e., $\hat{\mathbf{x}}$ is a shortest path with respect to \mathbf{c}^*) and 0 representing a perfectly discordant pathway (i.e., $\hat{\mathbf{x}}$ is a longest walk with respect to \mathbf{c}^* among all walks of at most the same number of steps as $\hat{\mathbf{x}}$).

THEOREM 2. *Given any feasible solution $\hat{\mathbf{x}}$ to the forward problem:*

1. $\omega(\hat{\mathbf{x}}) \in [0, 1]$,
2. $\omega(\hat{\mathbf{x}}) = 1$ if and only if $\mathbf{c}^* \hat{\mathbf{x}} = \mathbf{c}^* \mathbf{x}^*$,
3. $\omega(\hat{\mathbf{x}}) = 0$ if and only if $\hat{\mathbf{x}} \in \arg \max_{\mathbf{x}} \{\mathbf{c}^* \mathbf{x} : \mathbf{A} \mathbf{x} = \mathbf{b}, \mathbf{x} \geq \mathbf{0}, \|\mathbf{x}\|_1 \leq \|\hat{\mathbf{x}}\|_1, \mathbf{x} \text{ is a walk}\}$.

We end this section with a brief discussion on $M(\hat{\mathbf{x}})$. The denominator of $\omega(\hat{\mathbf{x}})$ normalizes the cost difference between the given pathway and an ideal pathway using the cost of the longest walk with length up to the length of $\hat{\mathbf{x}}$. Normalizing in this fashion implies that a longer walk could be, paradoxically, more concordant than a shorter walk, something that would not occur if the normalization term was a constant. However, we choose to normalize using $M(\hat{\mathbf{x}})$ for several reasons. First, this normalization allows the computation of $\omega(\hat{\mathbf{x}})$ to depend only on the given pathway $\hat{\mathbf{x}}$ (and \mathbf{c}^*) and not any other pathways. Normalizing by a fixed amount, M , while maintaining the property that $\omega(\hat{\mathbf{x}}) \geq 0$ for all $\hat{\mathbf{x}}$ would require that M be longer than all patient pathways that would be considered by $\omega(\hat{\mathbf{x}})$, an amount that could not be known a priori. Second, this approach aligns with common normalization approaches for edit distance metrics that are based on string length (Yujian and Bo 2007). Later, in our numerical results, we show that using $M(\hat{\mathbf{x}})$ results in an approximately normal distribution of $\omega(\hat{\mathbf{x}})$ for our dataset.

5. Application to Stage III Colon Cancer

In this section, we demonstrate the application of our inverse optimization framework to measure clinical pathway concordance, focusing on stage III colon cancer.

5.1. Problem Background

5.1.1. Disease Pathway Management at Cancer Care Ontario. The Disease Pathway Management (DPM) program at Cancer Care Ontario takes a systems view of setting priorities for cancer control, planning cancer services and improving the quality of cancer care in Ontario. DPM views patient journeys across the entire cancer continuum as part of an integrated process, as opposed to evaluating individual points of care in isolation. Clinicians are engaged to establish evidence-based best practices for the sequence of activities patients should take through the care network. These best practices are captured in *pathway maps* (Cancer Care Ontario 2019b), which reflect clinical guidelines for the care that patients should receive to optimize clinical outcomes. Pathway maps cover points of care spanning disease prevention, screening, diagnosis, treatment, recovery and end-of-life palliative care.

5.1.2. Stage III Colon Cancer and Pathway Map. Colon cancer is a malignant tumor of the colon. In 2018, roughly 180,000 people were diagnosed with colorectal cancer in North America and there were 64,000 deaths due to this cancer (World Health Organization 2019); colon cancer constitutes approximately 70% of the colorectal cancer cases (Colorectal Cancer Alliance 2019). Stage III colon cancer is characterized by metastasis of the cancer to the lymph nodes near the colon or by direct invasion into nearby organs. Chemotherapy is recommended as adjuvant therapy for surgically resected stage III disease. Twelve cycles of chemotherapy constitutes a complete treatment course.

The stage III colon cancer pathway map (Cancer Care Ontario 2019a) spans diagnosis and treatment, and contains the following major categories of activities: 1) clinical consultations, 2) endoscopy, 3) diagnostic imaging, 4) surgery, 5) adjuvant chemotherapy. Clinical consultations include consultations with a gastroenterologist (GI), surgeon and medical oncologist (MO). Diagnostic imaging includes imaging of the abdomen, pelvis and chest with any of the following modalities: computed tomography (CT), magnetic resonance imaging (MRI), ultrasound (US), or x-ray.

All concordant pathways must start with an endoscopy followed by abdominal imaging, chest imaging, surgical resection of the tumor, a MO consultation and finally chemotherapy. The patient will have had a GI or surgical consultation prior to the endoscopy, and a surgical consultation at some point before the surgical resection. Similarly, a MO consultation must occur before chemotherapy, preferably after the surgical resection. Abdominal imaging may take place as either an abdomen CT scan followed by a pelvis CT scan, or as an abdominal ultrasound. Similarly, chest

CT scans or chest x-rays constitute chest imaging. Chemotherapy is considered concordant if the patient pathway includes the recommended 12 treatment cycles. All of these different combinations are captured in the pathway map. Enumerating all of the possible concordant pathways from the pathway map results in 108 distinct reference pathways for stage III colon cancer.

5.2. Data

5.2.1. Data Sources. In Ontario, health care encounters are recorded in administrative databases using standardized methods. Using encrypted person-specific identifiers, we linked multiple sources to select the study population, define patient characteristics, and record activity related to screening, imaging, treatments, emergency department (ED) visits, and death. The data sources used in this study are listed in Appendix D.

5.2.2. Study Population. We developed a population-based cohort of individuals newly diagnosed with stage III colon cancer in 2010 in Ontario. Their clinical activities were recorded from six months prior to cancer diagnosis until either death or censoring at four years following diagnosis. Included patients had surgical resection within one year of diagnosis. Patients were excluded based on the following exclusion criteria: no Ontario health insurance number, residence outside of Ontario, non- incidental cancer diagnosis, any prior history of cancer or identification of a new primary cancer during the follow-up period, cancers diagnosed based on death records, unknown cancer stage, and unknown tumor histology. The final cohort contained 763 patients, 257 of whom died (from any cause) within the four-year post-diagnosis observation period.

The dataset is an event-log for each patient in the cohort describing the activities undertaken and their corresponding times relative to the date of diagnosis. However, not all events in the event-log are relevant to the diagnostic and treatment phases of care, which is our focus. Therefore we refine each patient's event-log by filtering out events earlier than 30 days prior to diagnosis and following one year post-diagnosis, since patients are expected to complete diagnostic and treatment activities within one year. If the patient completed chemotherapy (all 12 cycles) within the year, we remove all events after their last chemotherapy cycle. We also remove activities that have no bearing on concordance. For example, minor procedures like fecal occult blood tests and barium enemas were deemed inconsequential or extremely infrequent and were removed. All data refinements were implemented following consultations with clinicians.

5.3. Network Design

Next, we form a directed graph representing the clinical activity network based on activities from the pathway map, observed patient pathways, and discussions with clinical experts from the DPM team.

In clinical practice, GI, surgery and MO consultations always precede endoscopies, surgical resection and chemotherapy treatment, respectively. We therefore do not include nodes for these consultations in the graph and assume that they occur with the corresponding procedure. However, it is possible for patients to have additional consultations, which are costly for the system and deemed discordant. These discordant consultations, like visits to the emergency department, were quite prevalent in our dataset, so we included EXTRA CONSULT and ED VISIT as nodes in the graph. Another reason to include the latter is because reducing unnecessary visits to the ED is a Cancer Care Ontario priority.

Imaging events are distinct from consultations in that they are not implicit with other events, so we keep them as separate standalone activities. Imaging activities that were deemed functionally equivalent from a concordance perspective were merged into a single node. For example, abdomen MRI and ultrasound were combined into the node ABDOMEN MRI/US. We formed a single node for PELVIS MRI/US and CHEST IMAGING (which encompasses chest X-rays and CT scans) for the same reason. CT is preferred over the other imaging modalities for abdomen and pelvis, so we defined separate nodes for abdomen CT and pelvis CT.

Finally, our discussions with experts revealed that the type of treatment received by the patient should have extra bearing on their concordance score. To model the different possible ways each clinical or patient pathway can end, we include an “outcome layer” with four distinct nodes. Each pathway must exit the graph via one of these four nodes. Patients who receive 12 chemotherapy treatments exit through the node CHEMO COMPLETE. Receiving between 1 and 11 chemotherapy treatment cycles leads to an exit through the node CHEMO PARTIAL. The remaining pathways (no chemotherapy) exit either through the nodes MO CONSULT END (if the patient receives an MO consultation) or RESECTION END (if the patient does not). Recall that our patient cohort only includes patients who had surgical resection. The final network design used in our model is shown in Figure 1.

5.4. Inverse Optimization Model Specification

Since our final network design merged together several activities specified in the Cancer Care Ontario pathway map, the set of 108 reference pathways were reduced to two distinct reference pathways. One reference pathway is shown in Figure 1. The other reference pathway replaces ABDOMEN CT and PELVIS CT with ABDOMEN MRI/US. The network, reference pathways, survived patient pathways and died patient pathways constitute the (\mathbf{A}, \mathbf{b}) , $\hat{\mathcal{X}}^r := \{\hat{\mathbf{x}}_1^r, \hat{\mathbf{x}}_2^r\}$, $\hat{\mathcal{X}}^s$ and $\hat{\mathcal{X}}^d$, respectively, in formulations (1) and (3). The value of the (i, j) -th component of $\hat{\mathbf{x}}_q^r$ is 1 if reference pathway q includes arc (i, j) and 0 otherwise. Patient pathways are mapped to the graph similarly, except that each component of the vector represents the number of times that arc is

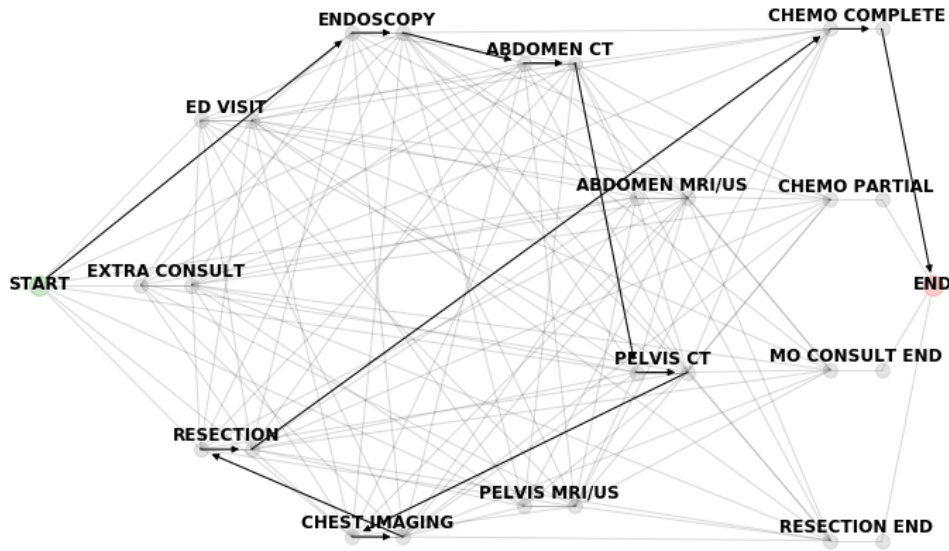


Figure 1 Stage III colon cancer clinical activity network with a reference pathway highlighted

traversed (which may be greater than one) in the patient pathway. Finally, with respect to \mathcal{C} , we included three sets of context-specific constraints on the imputed cost vector: 1) activity ranking constraints, 2) subpath constraints, and 3) penalty constraints.

Activity ranking constraints enforce a relative importance between pairs of activities. For example, clinical experts deemed ABDOMEN CT to be a more important activity than PELVIS CT. To account for this relationship in the model, we introduced a constraint that enforced the cost of completing ABDOMEN CT to be at most the cost of completing PELVIS CT (since it is a minimization problem). Specifically, if i represents ABDOMEN CT and j represents PELVIS CT, then the constraint would be $c_{i \rightarrow i} \leq c_{j \rightarrow j}$. There were eight such constraints in total between the nine non-outcome layer nodes.

Subpath rankings generalize activity ranking constraints to a sequence of nodes. For example, the subpath of ENDOSCOPY to ABDOMEN CT to PELVIS CT to CHEST IMAGING was preferred to the subpath of ENDOSCOPY to ABDOMEN MRI/US to CHEST IMAGING. Therefore, the sum of the arc costs along the first subpath (starting from the end node of ENDOSCOPY and ending with the start node of CHEST IMAGING) was constrained to be at most the sum of the arc costs along the second subpath. There were four such constraints in total. The first is the subpath ranking above. The remaining three rank the subpaths exiting the graph through the four outcome layer nodes, starting each subpath at RESECTION. In particular, the nodes in the outcome layer as depicted in Figure 1 are arranged from top to bottom in order of most preferred to least preferred outcome. For example, if i represents RESECTION, j represents RESECTION END, k represents MO CONSULT END, and E represents the final end node, then the subpath ranking between

RESECTION END and MO CONSULT END would be $c_{i_e j_s} + c_{j_s j_e} + c_{j_e E} \geq c_{i_e k_s} + c_{k_s k_e} + c_{k_e E}$. Similar subpath rankings were generated for MO CONSULT END versus CHEMO PARTIAL and CHEMO PARTIAL versus CHEMO COMPLETE.

Finally, since CHEMO COMPLETE is the best outcome node through which to exit the graph, we set the cost of the CHEMO COMPLETE to END arc to -1 , anchoring all the arc costs relative to this one. This constraint is also beneficial from a model tractability perspective. Recall that the inverse optimization model is solved via polyhedral decomposition, which amounts to solving several distinct optimization problems, each with a constraint of the form $c_{ij} = 1$ or $c_{ij} = -1$. Since we have an application-specific justification for setting one of the arc costs so that the constraint $\|\mathbf{c}\|_\infty = 1$ is automatically satisfied, we only need to solve a single optimization problem.

6. Inverse Optimization Results

We obtained an optimal cost vector, \mathbf{c}^* , by first solving formulation (1) followed by formulation (3) with the inputs described in Section 5.4. This cost vector comprises all arc costs and by definition minimizes the total suboptimality error of the two reference pathways, $\hat{\mathbf{x}}_1^r$ and $\hat{\mathbf{x}}_2^r$, and secondarily minimizes (maximizes) the suboptimality error of the patient pathways from survived (died) patients in $\hat{\mathcal{X}}^s$ ($\hat{\mathcal{X}}^d$). Figure 2 illustrates the \mathbf{c}^* values on the graph. Recall that since \mathbf{c}^* satisfies $\mathbf{A}\mathbf{c}^* = \mathbf{0}$, the sum of the costs on the incoming and outgoing arcs for each node are equal. As a consequence, the associated cost of passing through each node in the outcome layer is doubled, since each node in that layer has only one outgoing arc (i.e., the intra-activity arc (i_s, i_e) followed by the arc from the outcome node i_e to END).

Given the optimal cost vector \mathbf{c}^* , we found that $\rho_f(\hat{\mathcal{Z}}^r) = 1$. In other words, the duality gap associated with the two reference pathways was zero, indicating perfect model-data fit with the reference pathways. However, the average error from the patient pathways was positive, indicating that they are not shortest paths in general.

Finally, we calculated the concordance score of each patient pathway using (6) following a 10-fold cross-validation approach. The patient data was randomly partitioned into ten subsets (“folds”) that maintained the same class balance as the entire dataset. For each fold, the inverse optimization model was trained using the two reference pathways and 90% (nine of the subsets) of the patient data. The resulting cost vector was used in $\omega(\hat{\mathbf{x}})$ to measure the concordance of patient pathways in the out-of-sample 10% (the remaining subset). This process was carried out for all 10 folds and the distribution of out-of-sample concordance scores for the entire patient cohort is shown in Figure 3. The fact that this distribution is approximately normal stems from the choice of normalization in $\omega(\hat{\mathbf{x}})$. As Figure 4 shows, the distributions of the duality gap ϵ and pathway length $\|\hat{\mathbf{x}}\|_1$ are both skewed similarly, resulting in an approximately linear relationship between the two quantities. In

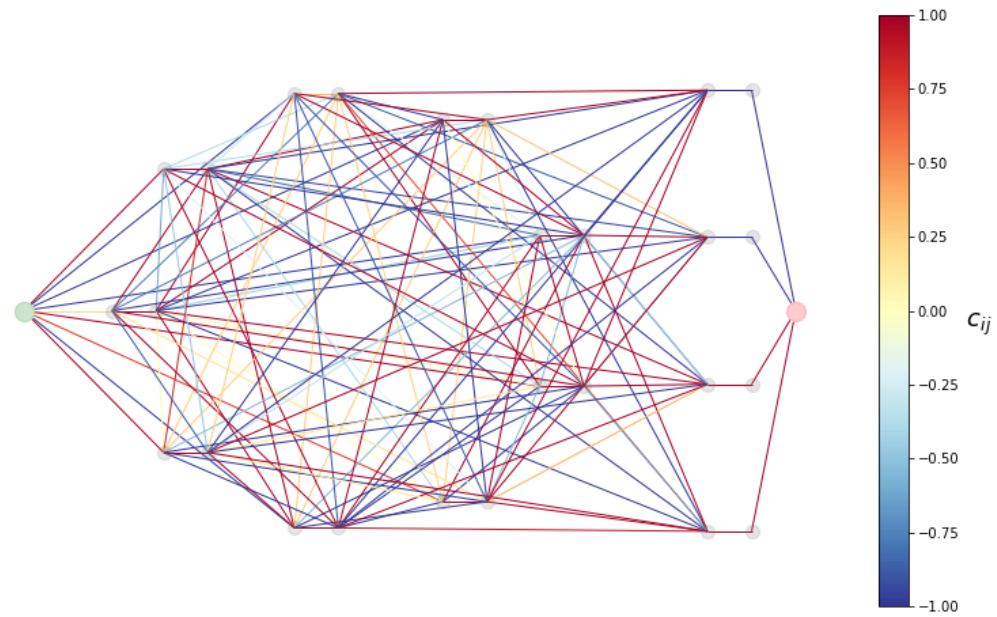


Figure 2 Stage III colon cancer clinical activity network with optimal cost vector overlaid

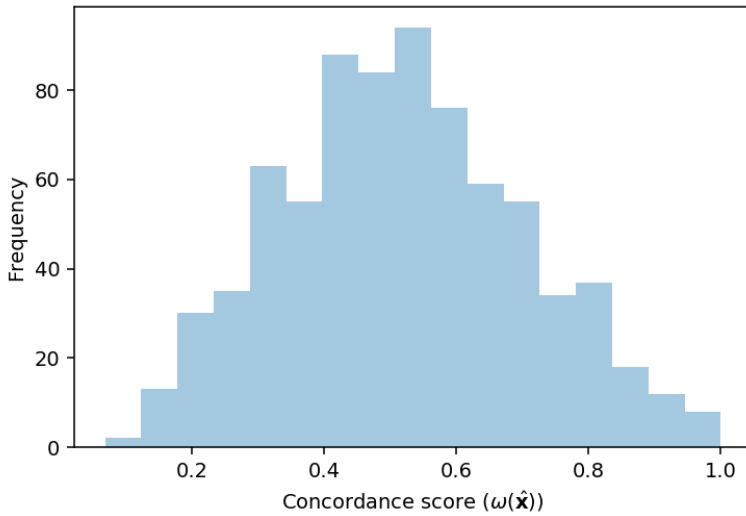


Figure 3 Distribution of concordance score over patient cohort

other words, the lack of fitness of a given patient pathway is associated with its corresponding length, and dividing one by the other creates the shape of the distribution seen in Figure 3.

As a crude analysis of association between concordance and survival, we generated smoothed cumulative distributions of the concordance scores, stratified by survival outcome, in Figure 5. Interestingly, the figure depicts first-order stochastic dominance, with a clear separation between patients who survived versus those who died. That is, for any given concordance score $\omega_0 \in [0, 1]$,

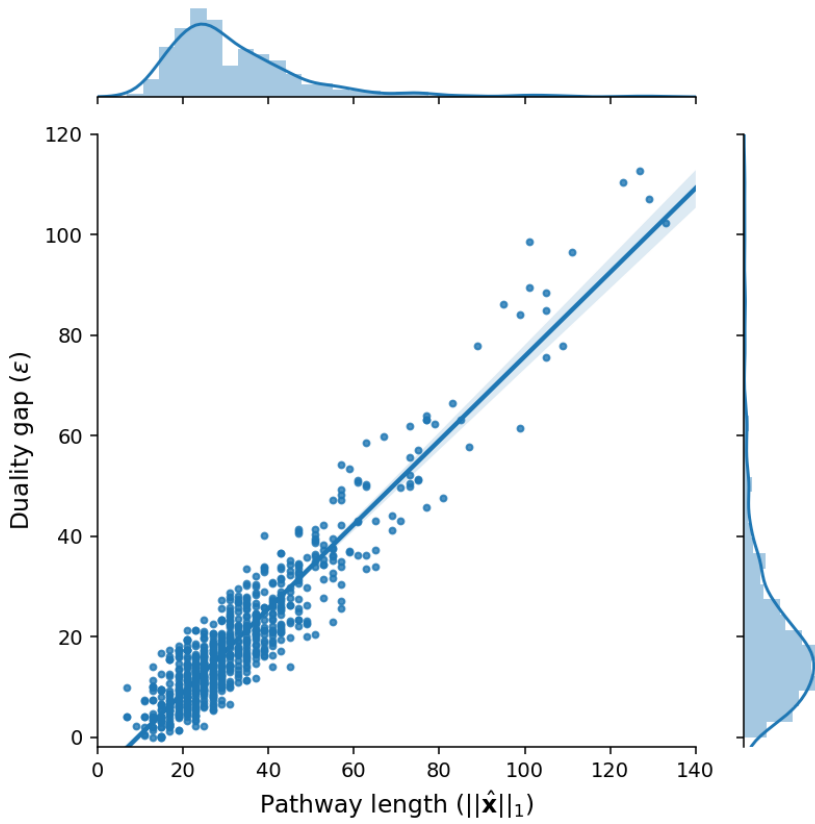


Figure 4 Relationship between duality gap and pathway length

the probability of scoring below ω_0 is higher for patients who died. Note that stochastic dominance is used in medical decision making to compare the costs or effectiveness of two or more distinct treatments (Leshno and Levy 2004, Sendi et al. 2003).

The results shown in Figure 5, while intuitive, do not provide a rigorous measure of the relationship between concordance and survival. Thus, in the next section, we perform a detailed survival analysis to establish the association between pathway concordance and survival.

7. Validating the Concordance Metric against Survival

7.1. Methods

For each patient in our study population, we obtained their characteristics as outlined in Section 5.2. Patient characteristics were summarized as counts with proportions for categorical data and means with standard deviations for continuous data. We binned the patient concordance scores into terciles and difference in covariate distributions among concordance score terciles was assessed with a chi-squared test for categorical variables and a one-way ANOVA for means and standard deviations. A Kaplan-Meier estimator was used for graphical presentation of (unadjusted) survival over time by the terciles of concordance scores. Difference in survival probabilities was assessed using the log-rank test statistic.

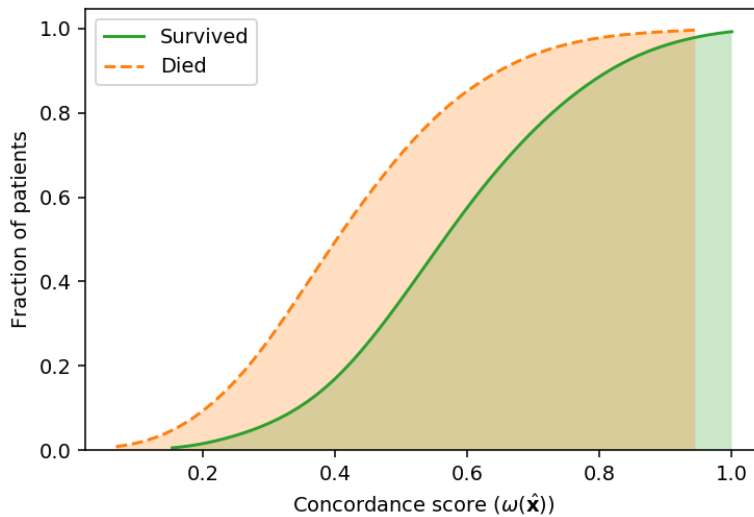


Figure 5 Cumulative distribution of concordance score over entire cohort stratified by patient outcome

A semi-parametric Cox proportional hazards model was implemented to evaluate the association between concordance scores and mortality (Cox 1971). Cox regression provides estimates of association between each variable and the hazard of event, i.e., the instantaneous rate of event. A unit increase in a covariate is multiplicative with respect to the hazard. An estimate of the hazard ratio (HR) above 1 indicates a variable that is positively associated with the risk of mortality, i.e., negatively associated with survival.

A range of known potential confounders and predictors of survival was assessed for inclusion in the model. These variables consist of demographic characteristics (age, sex, rural residency, quintiles of neighbourhood median income, terciles of immigrant population), Charlson comorbidity score (Charlson et al. 1987, Quan et al. 2005), cancer diagnostic and treatment characteristics (screening category, stage, tumor grade, emergent surgery status, length of hospital stay following the surgical treatment), and healthcare utilization a year prior to diagnosis (number of outpatient visits, presence of in-patient admissions, presence of ED visits), which is a proxy for overall patient health. Screening category refers to frequency and timing of blood tests (James et al. 2018). Stage specifies the cancer sub-stage, which denotes severity. The emergent surgery indicator refers to patients who had an urgent in-hospital admission when the surgical resection was performed.

We employed preliminary variable selection to control for important confounding effects while excluding covariates that would compromise model efficiency. Variable importance in predicting mortality was evaluated using an ensemble tree method for analysis of right-censored survival data (Ishwaran et al. 2008).

For the selected model, assumption of a linear relationship between a continuous independent variable and the outcome was evaluated by plotting the residuals against the covariate. If nonlinearity was detected either from the plots of Martingale residuals or Schoenfeld residuals, restricted cubic splines were used to model the continuous predictor (Stone and Koo 1985).

Variance of the estimated association between the concordance score and survival can increase in case of overfitting. Bootstrap model validation with 1000 resamples was performed to evaluate the degree of overfitting and potential overadjustment for confounders (Harrell Jr 2015).

Patients were excluded from the final survival model if they did not have all required covariate values, other than tumor grade, recorded. Patients who died within one year of diagnosis were also excluded, as they did not have the opportunity to complete their treatment journey in accordance with the clinical guidelines.

7.2. Results

A total of 665 individuals met the inclusion criteria for survival analysis. The mean age at diagnosis was 67.8 years (standard deviation = 13.2). Of the included patients, 165 (24.8%) died, with a higher proportion of deaths occurring among those with low concordance scores (38.5%, p-value < 0.0001).

Table 2 lists the characteristics of the entire cohort and by concordance terciles. Significant differences between the terciles were observed for age, rural residency, comorbidity score, health-care utilization, cancer stage, and characteristics related to cancer treatment. Sex, neighbourhood income and immigrant population, screening group, and tumor grade were not significantly different across terciles.

Table 2: Characteristics of stage III colon cancer cohort included in the survival analysis

Characteristic	Low (n=221)	Medium (n=222)	High (n=222)	Total (n=665)	p-value
Death, n (%)	85 (38.5)	49 (22.1)	31 (14.0)	165 (24.8)	<0.0001
Concordance score, mean (SD)	0.4 (0.1)	0.5 (0.0)	0.7 (0.1)	0.5 (0.2)	<0.0001
Patient characteristics					
Age at diagnosis, mean (SD)	74.0 (10.7)	65.9 (13.6)	63.4 (12.8)	67.8 (13.2)	<0.0001
Female, n (%)	121 (54.8)	119 (53.6)	101 (45.5)	341 (51.3)	0.1044
Rural residency, n (%)	39 (17.6)	22 (9.9)	25 (11.3)	86 (12.9)	0.0348
Neighbourhood Income Quintile, n (%)					
1 (lowest)	47 (21.3)	60 (27.0)	37 (16.7)	144 (21.7)	0.4321
2	40 (18.1)	42 (18.9)	44 (19.8)	126 (18.9)	
3	48 (21.7)	40 (18.0)	46 (20.7)	134 (20.2)	
4	46 (20.8)	42 (18.9)	53 (23.9)	141 (21.2)	
5 (highest)	40 (18.1)	38 (17.1)	42 (18.9)	120 (18.0)	

Cancer-related characteristics					
Screening group, n (%)					
None	118 (53.4)	120 (54.1)	109 (49.1)	347 (52.2)	0.5905
Repeated	12 (5.4)	16 (7.2)	12 (5.4)	40 (6.0)	
Diagnostic	31 (14.0)	34 (15.3)	30 (13.5)	95 (14.3)	
Sporadic	60 (27.1)	52 (23.4)	71 (32.0)	183 (27.5)	
Stage at diagnosis, n (%)					
IIIA (least advanced)	17 (7.7)	12 (5.4)	32 (14.4)	61 (9.2)	0.0191
IIIB	134 (60.6)	136 (61.3)	122 (55.0)	392 (58.9)	
IIIC (most advanced)	70 (31.7)	74 (33.3)	68 (30.6)	212 (31.9)	
Tumor Grade Category, n (%)					
Low	173 (78.3)	172 (77.5)	182 (82.0)	527 (79.2)	0.6545
High	40 (18.1)	40 (18.0)	30 (13.5)	110 (16.5)	
Unknown	8 (3.6)	10 (4.5)	10 (4.5)	28 (4.2)	
Emergent surgery, n (%)					
Length of in-hospital stay post surgery, mean (SD)	13.6 (17.0)	6.9 (4.7)	5.4 (2.1)	8.6 (10.8)	<0.0001
ED visits in the first year post diagnosis, n (%)	192 (86.9)	182 (82.0)	106 (47.7)	480 (72.2)	<0.0001
Number of ED visits post diagnosis, mean (SD)	2.9 (2.1)	2.3 (1.4)	1.7 (1.6)	2.4 (1.8)	<0.0001
Chemotherapy in the first year post diagnosis, n (%)					
Number of chemotherapy visits, mean (SD)	60 (27.1)	138 (62.2)	193 (86.9)	391 (58.8)	<0.0001
	9.5 (4.0)	10.9 (5.6)	11.3 (5.4)	10.9 (5.3)	0.0674

Statistically significant differences in (unadjusted) survival over time were observed for concordance score terciles (p-value < 0.0001, Figure 6).

Table 3 summarizes the association between concordance and survival for both unadjusted and adjusted Cox models with both categorical and continuous measures for the concordance score. The unadjusted Cox model found a significant effect of pathway concordance on survival, with decreased risk of mortality associated with having higher values of the concordance score in both the continuous (HR = 0.72, 95% CI = (0.66, 0.79)) and categorical models (HR = 0.51, 95% CI = (0.36, 0.73) for Medium vs. Low tercile; HR = 0.31, 95% CI = (0.20, 0.47) for High vs. Low

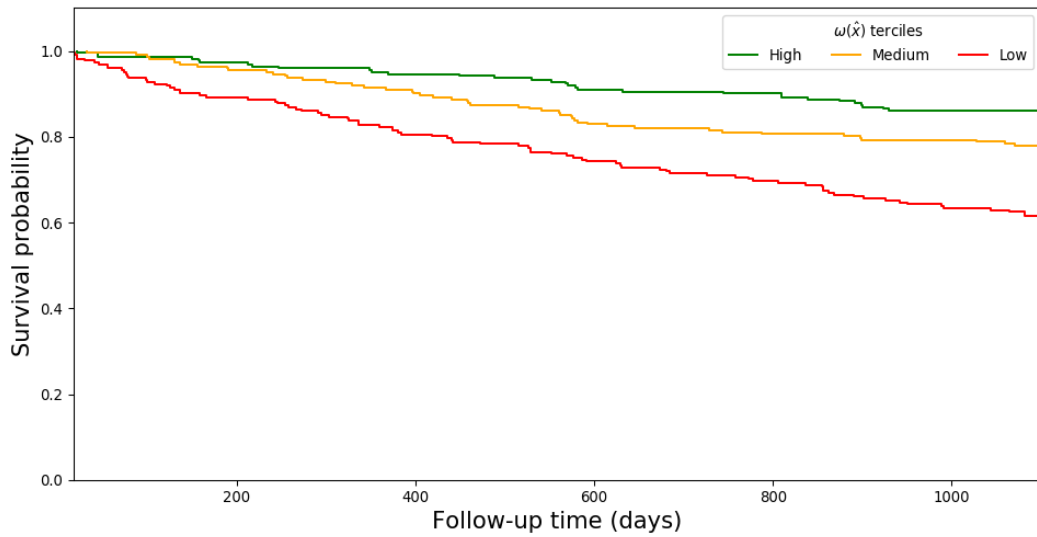


Figure 6 Kaplan-Meier curves for each concordance score tercile

Table 3 Risk of mortality associated with concordance score for categorical and continuous models

		Unadjusted			Adjusted		
		HR	95% CI	p-value	HR	95% CI	p-value
Categorical	ω (Med. vs Low)	0.51	(0.36, 0.73)	0.0002	0.70	(0.48, 1.03)	0.0684
	ω (High vs Low)	0.31	(0.20, 0.47)	<0.0001	0.57	(0.36, 0.92)	0.0216
Continuous	ω (unit change)	0.72	(0.66, 0.79)	<0.0001	0.80	(0.71, 0.90)	0.0003

tercile). Note that a unit change in the continuous model is scaled to represent a change of 0.1 in $\omega(\hat{\mathbf{x}})$.

Along with concordance score, the adjusted Cox regression included age, sex, rural residency, number of outpatient visits a year prior to diagnosis, screening group, cancer stage and grade, emergent surgery status, and length of hospital stay following the surgery. A nonlinear relationship between three covariates (age, number of outpatient visits, and length of hospital stay following the surgical treatment) was observed, so restricted cubic splines with three knots were used to model these covariates. No violation of model assumptions was detected. Results of the adjusted analyses showed statistical significance for the association between the concordance score and mortality. Similar to the unadjusted model, there was a significant effect of concordance on survival in the continuous model, with decreased risk of mortality associated with higher values of the concordance score (HR = 0.80, 95% CI = (0.71, 0.90)). However, only the High vs. Low tercile difference was significant (HR = 0.57, 95% CI = (0.36, 0.92)) for the categorical model.

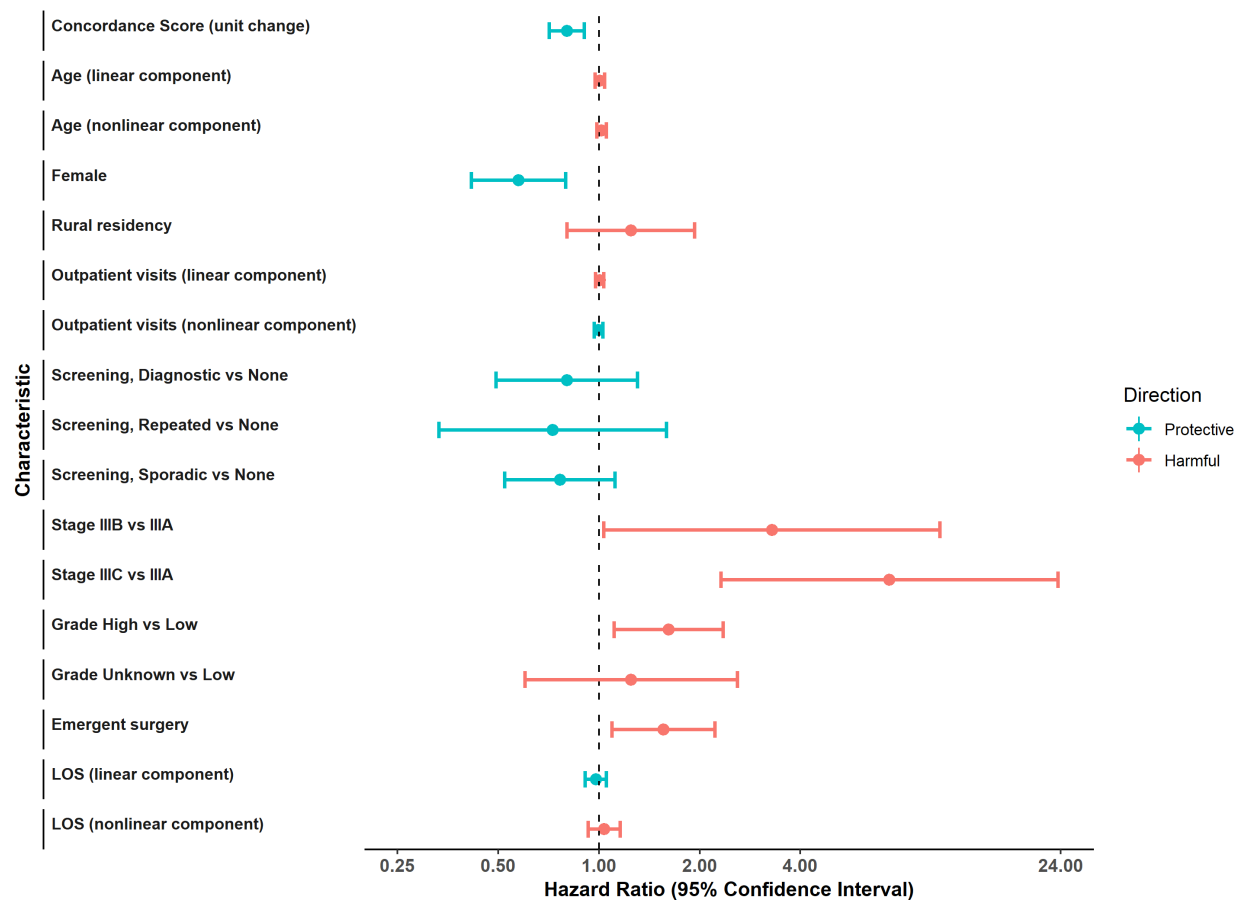


Figure 7 Forest plot of variable effects in continuous Cox regression model with 95% confidence intervals

Figure 7 summarizes the influence of each covariate in the adjusted continuous Cox model on survival. A hazard ratio below (above) 1 indicates a beneficial (harmful) effect on survival. If the confidence interval contains 1, the effect is not statistically significant at the 0.05 level. Concordance score and female sex have a statistically significant beneficial effect on survival, while cancer stage, cancer grade and emergent surgery have significant harmful effects. The corresponding figure for the adjusted categorical Cox model is provided in Appendix E.

Model validation with 1000 bootstrap resamples showed acceptable coefficient shrinkage (0.84) and model optimism (C-statistic reduction by 0.024), indicating minor evidence of overfitting. Based on the average of the bootstrap samples, we estimated a bias of -0.003 for the concordance score coefficient ($\log(\text{HR}) = -0.2207$ or $\text{HR} = 0.802$ in our model versus $\log(\text{HR}) = -0.2237$ or $\text{HR} = 0.799$ for the average of the bootstrap samples). The empirical confidence intervals of the concordance score estimates had similar coverage (0.70, 0.92) as the confidence intervals from the original model. The results of resampling imply model consistency in estimating the effect of the inverse optimization-based concordance score.

Table 4 Risk of mortality associated with concordance score for categorical and continuous models using the cost vector from reference pathway only model ($\mathbf{IO}^{\text{ref}}(\hat{\mathcal{X}}^r)$)

		Unadjusted			Adjusted		
		HR	95% CI	p-value	HR	95% CI	p-value
Categorical	ω (Med. vs Low)	0.66	(0.46, 0.94)	0.0215	1.07	(0.72, 1.60)	0.7239
	ω (High vs Low)	0.52	(0.36, 0.77)	0.0008	1.01	(0.65, 1.58)	0.9518
Continuous	ω (unit change)	0.75	(0.66, 0.86)	<0.0001	0.94	(0.81, 1.10)	0.4477

7.3. The Value of Patient Data

Finally, we repeat the above survival analysis using a cost vector (and associated concordance metric) that is derived from the model with only reference pathways as input ($\mathbf{IO}^{\text{ref}}(\hat{\mathcal{X}}^r)$) in order to quantify the value of our data-driven approach that uses patient pathway data to supplement the reference pathways. We focus on the Cox models (both categorical and continuous) and use the same methodological approach and dataset.

Table 4 summarizes the association between concordance and survival based on the reference-only cost vector. Similar to the data-driven approach, the unadjusted Cox model found a significant effect of pathway concordance on survival in both the continuous (HR = 0.75, 95% CI = (0.66, 0.86)) and categorical models (HR = 0.66, 95% CI = (0.46, 0.94) for Medium vs. Low tercile; HR = 0.52, 95% CI = (0.36, 0.77) for High vs. Low tercile). However, after adjusting for other relevant covariates, the association weakened significantly. In particular, there is no longer any significant association between concordance score and survival for both the categorical or continuous models. For illustrative purposes, we include the forest plot for only the continuous model in Appendix E.

Overall, this analysis shows that a data-driven approach, using patient data to refine the cost vector so alignment with patient outcomes is improved, produces a pathway concordance metric that is much more relevant and statistically meaningful for population-based health outcome monitoring.

8. Conclusions

This paper proposes the first data-driven inverse optimization approach to measuring pathway concordance in any problem context. Our specific development focuses on clinical pathway concordance for cancer patients. We model the care network as a directed graph and use both recommended pathways and actual patient pathways to develop and refine a novel pathway concordance metric. We confirm the value of our data-driven approach by showing that the concordance scores are strongly associated with survival for patients with stage III colon cancer, even after adjusting for other patient covariates.

In contrast to previous work in clinical pathway concordance, which focus on single events or courses of treatment by patients in a single institution, our concordance score can support population-level health system monitoring and reporting. Given its statistically significant association with clinical outcomes, our metric provides meaningful quantitative measures of system efficiency and variation. Improving concordance measurement in a data-driven and generalizable manner allows officials to evaluate complex practice patterns at the population level and describe clinical (e.g., survival) and system (e.g., cost) outcomes in relation to variation in care. These rich data can then be explored for providing decision support to clinicians and health system administrators. Measuring pathway concordance may help identify gaps and bottlenecks in the health system, facilitate modeling of system changes and resulting costs, and allow for inter-jurisdictional comparison while accommodating system differences. These activities, in turn, can help support planning and priority setting. Concordance metrics optimized for clinical outcomes are also useful in promoting and implementing best practice, helping providers focus on appropriate interventions and reduce inappropriate resource use. These topics are the focus of future work, where concordance measurement will be explored to identify opportunities for improvement along the entire care continuum and among different patient populations.

Our methodological contribution includes a two-stage inverse optimization approach to handling primary and secondary data sources, as well as a model that tries to separate good and bad (secondary) data points as much as possible. These methodological advances, motivated by our real-world problem context, suggest avenues for future research in inverse optimization. To keep our models tractable, temporal aspects of concordance measurement were accounted for in how we processed the event logs to form patient pathways. Future work may also consider modifying the clinical activity network so the state space captured by the nodes also include temporal characteristics, such as receipt of treatment before or after a certain time frame.

Appendix A: Proofs

Proof of Lemma 1. Since the objective function has a lower bound of zero, it suffices to show that $\mathbf{IO}^{\text{ref}}(\hat{\mathcal{X}}^r)$ is feasible if and only if there are at least two distinct paths from the start node (denoted s) to the end node (denoted t).

(\Leftarrow) Let P_1 and P_2 be two distinct paths from s to t . Let $P_1 \setminus P_2 = \{(i, j) \in \mathcal{A} \mid (i, j) \in P_1 \text{ and } (i, j) \notin P_2\}$ and $P_2 \setminus P_1 = \{(i, j) \in \mathcal{A} \mid (i, j) \in P_2 \text{ and } (i, j) \notin P_1\}$. If we set $c_{ij} = -1$ for $(i, j) \in P_1 \setminus P_2$, $c_{ij} = 1$ for $(i, j) \in P_2 \setminus P_1$, and $c_{ij} = 0$ for all the other arcs in the network, then \mathbf{c} satisfies $\|\mathbf{c}\|_\infty = 1$ and $\mathbf{A}\mathbf{c} = \mathbf{0}$. Note that P_1 is the shortest path for the designed cost vector \mathbf{c} which has finite total cost. From strong duality, its dual is also optimal meaning that there exists a \mathbf{p} that satisfies constraint $\mathbf{A}'\mathbf{p} \leq \mathbf{c}$ for \mathbf{c} . Finally, we build a feasible solution for $\mathbf{IO}^{\text{ref}}(\hat{\mathcal{X}}^r)$ by setting $\epsilon_q^r = \mathbf{c}'\hat{\mathbf{x}}_q^r - \mathbf{b}'\mathbf{p}$ for $q = 1, \dots, R$.

(\Rightarrow) Suppose to the contrary that there is only one path from s to t , which means the entire network itself

is the path from s to t . Since there is a feasible \mathbf{c} , there is some arc (i, j) with cost $|\mathbf{c}_{ij}| = 1$. The constraint $\mathbf{Ac} = \mathbf{0}$ implies that the incoming arc to i and outgoing arc from j also has cost equal to 1 in absolute value. Continuing this logic, the same will be true of the outgoing arc from s , but this violates $\mathbf{Ac} = \mathbf{0}$, meaning \mathbf{c} cannot be feasible. \square

Proof of Proposition 1. The dual of $\mathbf{FO}(\mathbf{c}^*)$ is feasible since \mathbf{c}^* and \mathbf{p}^* satisfy the dual feasibility conditions. Hence, $\mathbf{FO}(\mathbf{c}^*)$ is not unbounded, implying no negative cost cycles. \square

Proof of Proposition 2. Let $(\mathbf{c}^*, \mathbf{p}^*, \boldsymbol{\epsilon}^{r*})$ be an optimal solution to $\mathbf{IO}^{\text{ref}}(\hat{\mathcal{X}}^r)$. We can construct a feasible solution to $\mathbf{IO}^{\text{pat}}(\hat{\mathcal{X}}^s, \hat{\mathcal{X}}^d, \boldsymbol{\epsilon}^{r*})$ by setting $\epsilon_q^s = \mathbf{c}^{*'} \hat{\mathbf{x}}_q^s - \mathbf{b}' \mathbf{p}^*$ for $q = 1, \dots, S$ and $\epsilon_q^d = \mathbf{c}^{*'} \hat{\mathbf{x}}_q^d - \mathbf{b}' \mathbf{p}^*$ for $q = 1, \dots, D$. Hence, what remains is to show that the objective is bounded. Substituting the third and fourth constraints into the objective, we have

$$\begin{aligned} \frac{D}{S} \sum_{q=1}^S \epsilon_q^s - \sum_{q=1}^D \epsilon_q^d &= \frac{D}{S} \left(\sum_{q=1}^S \mathbf{c}' \hat{\mathbf{x}}_q^s - S \mathbf{b}' \mathbf{p} \right) - \left(\sum_{q=1}^D \mathbf{c}' \hat{\mathbf{x}}_q^d - D \mathbf{b}' \mathbf{p} \right) \\ &= \frac{D}{S} \sum_{q=1}^S \mathbf{c}' \hat{\mathbf{x}}_q^s - \sum_{q=1}^D \mathbf{c}' \hat{\mathbf{x}}_q^d, \end{aligned}$$

which is clearly bounded below since $\hat{\mathbf{x}}_q^s$ and $\hat{\mathbf{x}}_q^d$ are data and $\|\mathbf{c}\|_\infty = 1$. In particular, if $M = \max_{q,q'} \{\|\hat{\mathbf{x}}_q^s\|, \|\hat{\mathbf{x}}_{q'}^d\|\}$, then by Holder's inequality the absolute value of the objective is bounded by $2DM$. \square

Proof of Theorem 1. 1. Given $\hat{\mathcal{X}}^r$ and $\mathbf{c}_t, t = 1, \dots, T$, the denominator term in $\rho(\hat{\mathcal{X}}^r)$ is fixed. An optimal solution to $\mathbf{IO}^{\text{ref}}(\hat{\mathcal{X}}^r)$, by definition of its objective function, minimizes the numerator of $1 - \rho(\hat{\mathcal{X}}^r)$, thus maximizing $\rho(\hat{\mathcal{X}}^r)$.

2. It is clear that $\rho(\hat{\mathcal{X}}^r) \leq 1$ since $1 - \rho(\hat{\mathcal{X}}^r)$ is the ratio of sums of squares, which are nonnegative. To show $\rho(\hat{\mathcal{X}}^r) \geq 0$, note that $\sum_{q=1}^R (\mathbf{c}^{*'} \hat{\mathbf{x}}_q^r - \mathbf{c}^{*'} \mathbf{x}^*)^2 \leq \sum_{q=1}^R (\mathbf{c}'_t \hat{\mathbf{x}}_q^r - \mathbf{c}'_t \mathbf{x}_t)^2$ for all t because \mathbf{c}_t is a feasible solution to $\mathbf{IO}^{\text{ref}}(\hat{\mathcal{X}}^r)$.

3. An optimal solution to $\mathbf{IO}_{(k)}^{\text{ref}}(\hat{\mathcal{X}}^r)$ is feasible for $\mathbf{IO}_{(k+1)}^{\text{ref}}(\hat{\mathcal{X}}^r)$, since the latter problem is a relaxation of the former. Invoking the first statement in this theorem, $\rho_{(k)}(\hat{\mathcal{X}}^r) \leq \rho_{(k+1)}(\hat{\mathcal{X}}^r)$. \square

Proof of Theorem 2. Note that $M(\hat{\mathbf{x}}) \geq \mathbf{c}^{*'} \hat{\mathbf{x}} \geq \mathbf{c}^{*'} \mathbf{x}^*$, where the first inequality is by definition of $M(\hat{\mathbf{x}})$ and second inequality is by optimality of \mathbf{x}^* . It is straightforward to then show that $0 \leq \omega(\hat{\mathbf{x}}) \leq 1$, with equality at the lower or upper bound when the first or second inequalities above on $\mathbf{c}^{*'} \hat{\mathbf{x}}$, respectively, are tight. \square

Appendix B: Lower-Dimensional Transformation for ρ Calculation

Because $m < n$ and $\mathbf{A} \in \mathbb{R}^{(m-1) \times n}$ has rank $m - 1$, we can partition \mathbf{A} to two matrices \mathbf{B} and \mathbf{N} in which \mathbf{B} is a square matrix comprising the linear independent columns of \mathbf{A} while \mathbf{N} comprises the remaining columns of \mathbf{A} (Bertsekas 1999). We denote the corresponding decomposition of \mathbf{x} and \mathbf{c} by $[\mathbf{x}_B; \mathbf{x}_N]$ and $[\mathbf{c}_B; \mathbf{c}_N]$, respectively. Substituting $\mathbf{x}_B = \mathbf{B}^{-1}(\mathbf{b} - \mathbf{N}\mathbf{x}_N)$ in the shortest path problem transforms the feasible region to a lower dimensional space where $\mathbf{z} = \mathbf{x}_N \in \mathbb{R}^{n-(m-1)}$ is the variable, and the feasible region is represented by inequality constraints only: $\min_{\mathbf{z}} \{\mathbf{d}' \mathbf{z} + C : \mathbf{B}^{-1} \mathbf{N} \mathbf{z} \leq \mathbf{B}^{-1} \mathbf{b}, \mathbf{z} \geq \mathbf{0}\}$ where $\mathbf{d} = \mathbf{c}_N - \mathbf{c}_B \mathbf{B}^{-1} \mathbf{N}$ and $C = \mathbf{c}_B \mathbf{B}^{-1} \mathbf{b}$. The transformed problem is a full-dimensional problem in dimension $n - (m - 1)$.

Appendix C: Calculation of Longest Walk Length $M(\hat{\mathbf{x}})$

We use the Bellman-Ford equations to calculate the longest walk for walks up to a given length N . Let the node set be \mathcal{N} , the start node be s , and the end node be t . Let $C(v, k)$ be the cost of the longest walk from s to $v \in \mathcal{N}$ that takes k steps, computed via backward induction over the equations

$$\begin{aligned} C(v, k) &= \max_{u \in \mathcal{N}} \{C(u, k-1) + c(u, v)\}, \quad k = 2, \dots, N, \quad v \in \mathcal{N}, \\ C(s, 1) &= 0, \\ C(v, 1) &= \infty, \quad v \neq s, \end{aligned}$$

where $c(u, v) = c_{uv}$ if $(u, v) \in \mathcal{A}$, and $c(u, v) = \infty$ otherwise. We solve this system of equations once up to a value of N that equals the length of the longest patient pathway ($\max_{q, q'} \{\|\hat{\mathbf{x}}_q^s\|, \|\hat{\mathbf{x}}_{q'}^d\|\}$). Then, the costs of the longest walks with length for each integer up to N are stored and can simply be looked up when computing $\omega(\hat{\mathbf{x}})$ for each patient pathway.

Appendix D: Data Sources

- Cancer Care Ontario
 - Ontario Cancer Registry (OCR)
 - Collaborative Stage Dataset (CSI)
 - Colonoscopy Interim Reporting Tool (CIRT)
 - Lab Reporting Tool (LRT)
 - Screening HUB
 - Activity Level Reporting (ALR)
- Ministry of Health and Long-Term Care (MoHLTC)
 - Registered Persons Database (RPDB)
 - Ontario Health Insurance Plan (OHIP) Claims
- Canadian Institute for Health Information (CIHI)
 - National Ambulatory Care Reporting System (NACRS)
 - Discharge Abstract Database (DAD)
- Statistics Canada
 - Postal Code Conversion file (PCCF+6B)

Appendix E: Supplementary Figures for Survival Analysis

Figure 8 summarizes the influence of each covariate in the adjusted categorical Cox model from Section 7.2 on survival. Figure 9 depicts a similar forest plot, but for the adjusted continuous Cox model with the concordance score based on the reference pathway-only model from Section 7.3.

References

Adriansyah A, van Dongen BF, van der Aalst WM (2011) Conformance checking using cost-based fitness analysis. *Enterprise Distributed Object Computing Conference (EDOC), 2011 15th IEEE International*, 55–64 (IEEE).

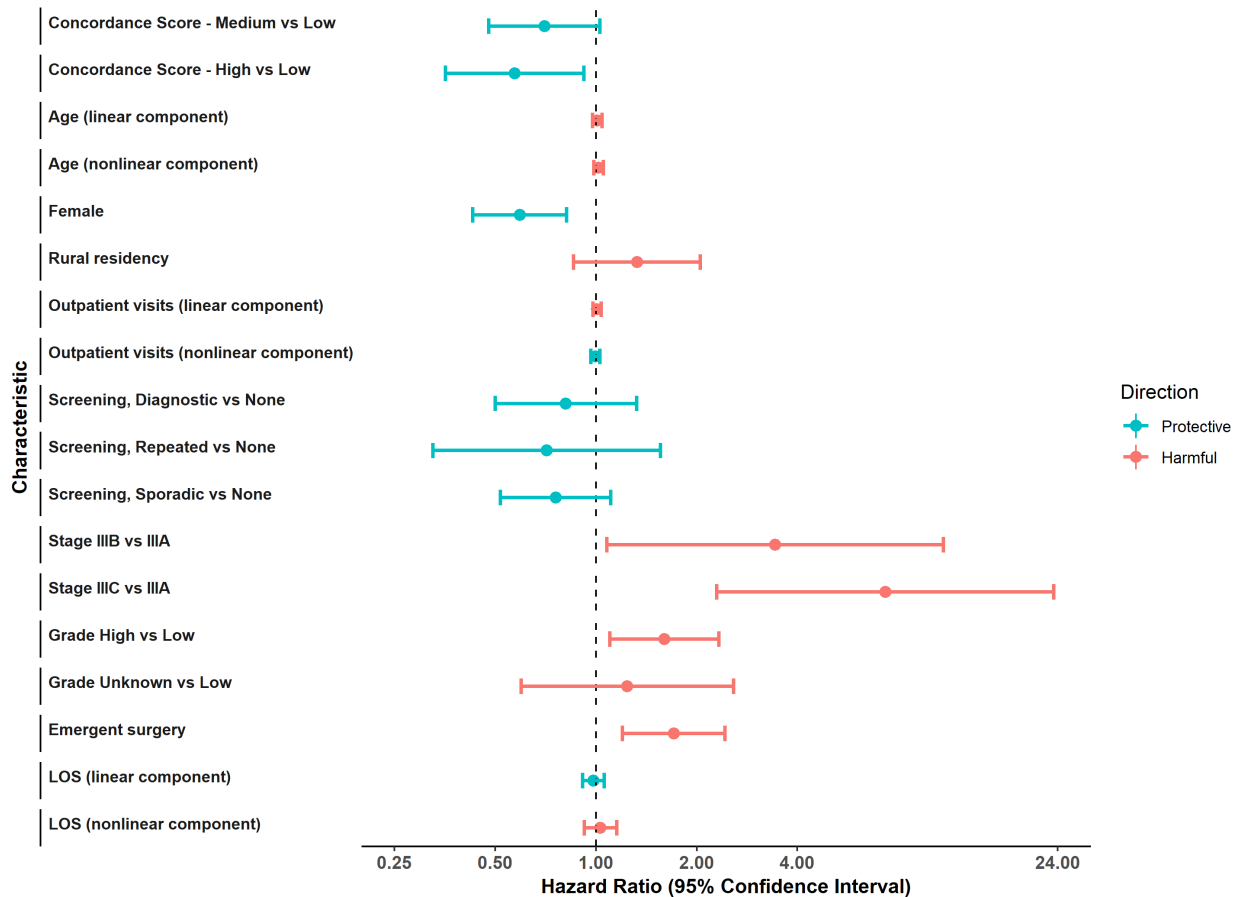


Figure 8 Forest plot of variable effects in categorical Cox regression model with 95% confidence intervals

Ahuja RK, Orlin JB (2001) Inverse optimization. *Operations Research* 49(5):771–783.

Ahuja RK, Orlin JB (2002) Combinatorial algorithms for inverse network flow problems. *Networks: An International Journal* 40(4):181–187.

Aswani A, Shen ZJ, Siddiq A (2018) Inverse optimization with noisy data. *Operations Research* 66(3):870–892.

Babier A, Chan TC, Lee T, Mahmood R, Terekhov D (2019) A unified framework for model fitting and evaluation in inverse linear optimization. *arXiv preprint arXiv:1804.04576v2* .

Bertsekas D (1999) *Nonlinear Programming* (Athena Scientific), 2 edition, ISBN 1-886529-00-0.

Bertsimas D, Gupta V, Paschalidis IC (2015) Data-driven estimation in equilibrium using inverse optimization. *Mathematical Programming* 153(2):595–633.

Bose RJC, van der Aalst W (2010) Trace alignment in process mining: opportunities for process diagnostics. *International Conference on Business Process Management*, 227–242 (Springer).

Burton D, Pulleyblank W, Toint PL (1997) The inverse shortest paths problem with upper bounds on shortest paths costs. *Network Optimization*, 156–171 (Springer).

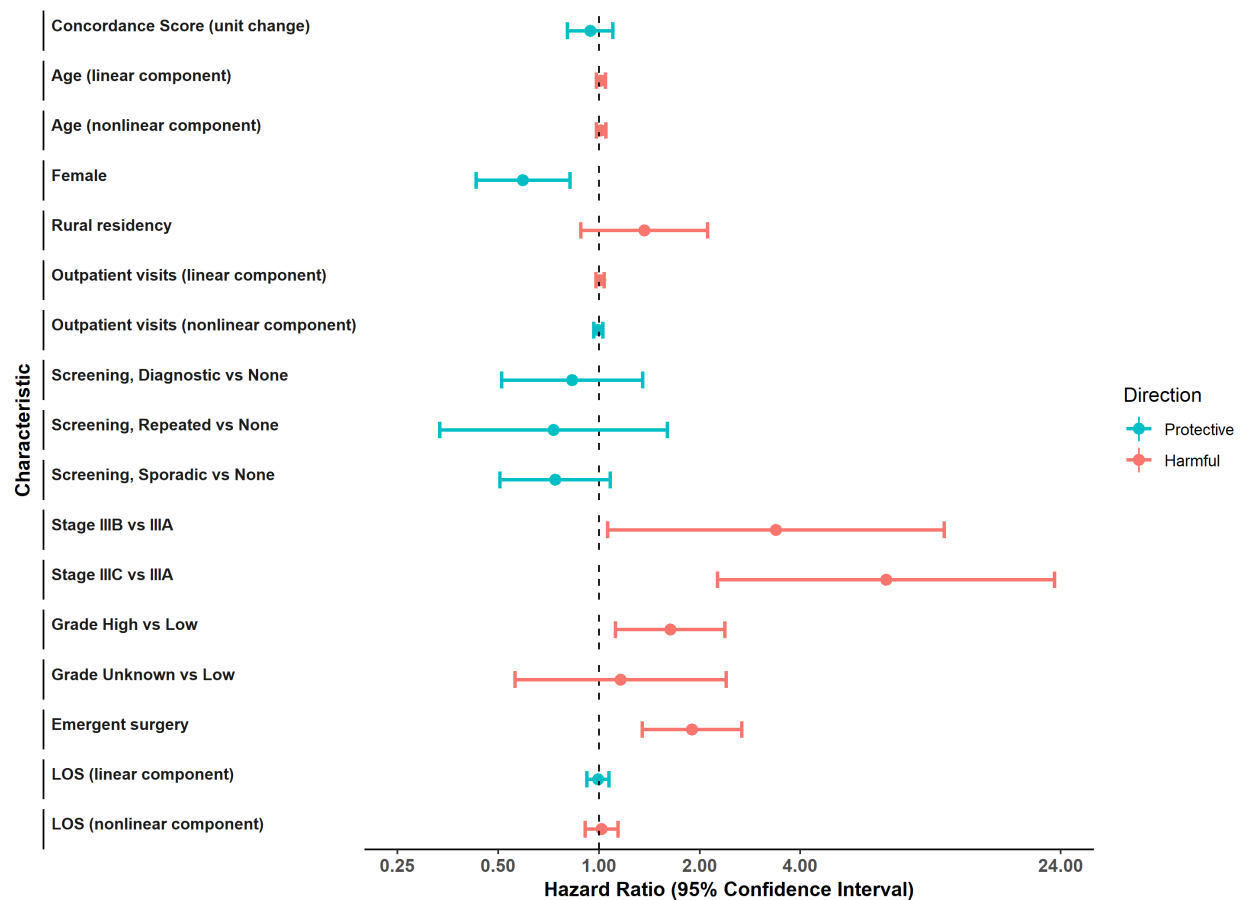


Figure 9 Forest plot of variable effects in continuous Cox regression model with 95% confidence intervals using concordance score based only on reference pathway data

Burton D, Toint PL (1992) On an instance of the inverse shortest paths problem. *Mathematical Programming* 53(1-3):45–61.

Campbell H, Hotchkiss R, Bradshaw N, Porteous M (1998) Integrated care pathways. *Bmj* 316(7125):133–137.

Cancer Care Ontario (2019a) Colorectal cancer pathway map. URL <https://www.cancercareontario.ca/en/pathway-maps/colorectal-cancer>.

Cancer Care Ontario (2019b) Pathway maps. URL <https://www.cancercareontario.ca/en/pathway-maps>.

Chan TC, Craig T, Lee T, Sharpe MB (2014) Generalized inverse multiobjective optimization with application to cancer therapy. *Operations Research* 62(3):680–695.

Chan TC, Lee T, Terekhov D (2019) Inverse optimization: Closed-form solutions, geometry, and goodness of fit. *Management Science* 65(3):1115–1135.

Charlson ME, Pompei P, Ales KL, MacKenzie CR (1987) A new method of classifying prognostic comorbidity in longitudinal studies: development and validation. *Journal of chronic diseases* 40(5):373–383.

Colorectal Cancer Alliance (2019) Determine your risk and practice prevention. URL <https://www.ccalliance.org/colorectal-cancer-information/statistics-risk-factors>.

Cox D (1971) Regression models and life-tables (with discussion). *Journal of the Royal Statistical Society* 34(2):187–220.

Esfahani PM, Shafieezadeh-Abadeh S, Hanasusanto GA, Kuhn D (2018) Data-driven inverse optimization with imperfect information. *Mathematical Programming* 167(1):191–234.

Evans WK, Ung YC, Assouad N, Chyrek A, Sawka C (2013) Improving the quality of lung cancer care in ontario: the lung cancer disease pathway initiative. *Journal of Thoracic Oncology* 8(7):876–882.

Faragó A, Szentesi Á, Szviatovszki B (2003) Inverse optimization in high-speed networks. *Discrete Applied Mathematics* 129(1):83–98.

Forestier G, Lalys F, Riffaud L, Trelhu B, Jannin P (2012) Classification of surgical processes using dynamic time warping. *Journal of biomedical informatics* 45(2):255–264.

Gao X, Xiao B, Tao D, Li X (2010) A survey of graph edit distance. *Pattern Analysis and applications* 13(1):113–129.

Harrell Jr FE (2015) *Regression modeling strategies: with applications to linear models, logistic and ordinal regression, and survival analysis* (Springer).

Ishwaran H, Kogalur UB, Blackstone EH, Lauer MS, et al. (2008) Random survival forests. *The annals of applied statistics* 2(3):841–860.

James PD, Rabeneck L, Yun L, Paszat L, Baxter NN, Govindarajan A, Antonova L, Timmou JM (2018) Repeated faecal occult blood testing is associated with decreased advanced colorectal cancer risk: A population-based study. *Journal of medical screening* 25(3):141–148.

Keshavarz A, Wang Y, Boyd S (2011) Imputing a convex objective function. *Intelligent Control (ISIC), 2011 IEEE International Symposium on*, 613–619 (IEEE).

Leshno M, Levy H (2004) Stochastic dominance and medical decision making. *Health Care Management Science* 7(3):207–215.

Ling DC, Karukonda P, Smith RP, Heron DE, Beriwal S (2018) Declining brachytherapy utilization for high-risk prostate cancer - can clinical pathways reverse the trend? *Brachytherapy* 17(6):895–898.

Navarro G (2001) A guided tour to approximate string matching. *ACM computing surveys (CSUR)* 33(1):31–88.

Neuhaus M, Bunke H (2004) A probabilistic approach to learning costs for graph edit distance. *Proceedings of the 17th International Conference on Pattern Recognition, 2004. ICPR 2004.*, volume 3, 389–393 (IEEE).

Panella M, Marchisio S, Di Stanislao F (2003) Reducing clinical variations with clinical pathways: do pathways work? *International Journal for Quality in Health Care* 15(6):509–521.

Quan H, Sundararajan V, Halfon P, Fong A, Burnand B, Luthi JC, Saunders LD, Beck CA, Feasby TE, Ghali WA (2005) Coding algorithms for defining comorbidities in icd-9-cm and icd-10 administrative data. *Medical care* 43(11):1130–1139.

Riesen K (2015) Structural pattern recognition with graph edit distance. *Advances in computer vision and pattern recognition, Cham* .

Ristad ES, Yianilos PN (1998) Learning string-edit distance. *IEEE Transactions on Pattern Analysis and Machine Intelligence* 20(5):522–532.

Rotter T, Kinsman L, James E, Machotta A, Willis J, Snow P, Kugler J (2012) The effects of clinical pathways on professional practice, patient outcomes, length of stay, and hospital costs: Cochrane systematic review and meta-analysis. *Evaluation & the health professions* 35(1):3–27.

Samokhvalov AV, Probst C, Awan S, George TP, Le Foll B, Voore P, Rehm J (2018) Outcomes of an integrated care pathway for concurrent major depressive and alcohol use disorders: a multisite and prospective study. *BMC Psychiatry* 18(189).

Schmidt I, Thor J, Davidson T, Nilsson F, Carlsson C (2018) The national program on standardized cancer care pathways in sweden: Observations and findings halfway through. *Health Policy* 122(9):945–948.

Sendi P, Al MJ, Gafni A, Birch S (2003) Optimizing a portfolio of health care programs in the presence of uncertainty and constrained resources. *Social Science & Medicine* 57(11):2207–2215.

Stone CJ, Koo CY (1985) Additive splines in statistics. *Proceedings of the American Statistical Association. Original pagination is p 45:48.*

Troutt MD, Pang WK, Hou SH (2006) Behavioral estimation of mathematical programming objective function coefficients. *Management science* 52(3):422–434.

van de Klundert J, Gorissen P, Zeemering S (2010) Measuring clinical pathway adherence. *Journal of biomedical informatics* 43(6):861–872.

Van Zelm R, Janssen I, Vanhaecht K, de Buck van Overstraeten A, Panella M, Sermeus W, Coeckelberghs E (2018) Development of a model care pathway for adults undergoing colorectal cancer surgery: Evidence-based key interventions and indicators. *Journal of evaluation in clinical practice* 24(1):232–239.

World Cancer Research Fund (2019) Colorectal cancer statistics: Colorectal cancer is the third most common cancer worldwide. URL <https://www.wcrf.org/dietandcancer/cancer-trends/colorectal-cancer-statistics>.

World Health Organization (2019) Colorectal cancer. URL https://gco.iarc.fr/today/data/factsheets/cancers/10_8_9-Colorectum-fact-sheet.pdf?fbclid=IwAR3xpp3qDLrfrCAKXjR1XAM-6HUZZYpUPqk8kvaY6llk5eyAs1CrZ4k0Me4.

Xu S, Zhang J (1995) An inverse problem of the weighted shortest path problem. *Japan journal of industrial and applied mathematics* 12(1):47.

Yan H, Van Gorp P, Kaymak U, Lu X, Ji L, Chiau CC, Korsten HH, Duan H (2018) Aligning event logs to task-time matrix clinical pathways in bpmn for variance analysis. *IEEE Journal of Biomedical and Health Informatics* 22(2):311–317.

Yang C, Zhang J, Ma Z (1997) Inverse maximum flow and minimum cut problems. *Optimization* 40(2):147–170.

Yang S, Dong X, Sun L, Zhou Y, Farneth RA, Xiong H, Burd RS, Marsic I (2017) A data-driven process recommender framework. *Proceedings of the 23rd ACM SIGKDD International Conference on Knowledge Discovery and Data Mining*, 2111–2120 (ACM).

Yang S, Zhou M, Webman R, Yang J, Sarcevic A, Marsic I, Burd RS (2016) Duration-aware alignment of process traces. *Industrial Conference on Data Mining*, 379–393 (Springer).

Yujian L, Bo L (2007) A normalized levenshtein distance metric. *IEEE transactions on pattern analysis and machine intelligence* 29(6):1091–1095.

Zhang J, Cai MC (1998) Inverse problem of minimum cuts. *Mathematical Methods of Operations Research* 47(1):51–58.

Zhang J, Ma Z (1996) A network flow method for solving some inverse combinatorial optimization problems. *Optimization* 37(1):59–72.

Zhang J, Ma Z, Yang C (1995) A column generation method for inverse shortest path problems. *Zeitschrift für Operations Research* 41(3):347–358.

Zhao Q, Stettner A, Reznik E, Segrè D, Paschalidis IC (2015) Learning cellular objectives from fluxes by inverse optimization. *Decision and Control (CDC), 2015 IEEE 54th Annual Conference on*, 1271–1276 (IEEE).